AD-A165 464 TRANSIENT TRANSPORT IN BINARY AND TERNARY SEMICONDUCTORS(U) SCIENTIFIC RESEARCH ASSOCIATES INC GLASTONBURY CT H L GRUBIN ET AL. 27 FEB 86 1/1

UNCLASSIFIED SRA-R930009-F ARO-18480.5-EL F/G 20/12 NL

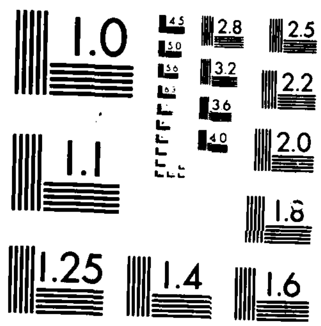

MICROCOPY RESOLUTION TEST CHART

TRANSIENT TRANSPORT IN BINARY AND TERNARY SEMICONDUCTORS

FINAL REPORT - R930009-F

H.L. GRUBIN
J.P. KRESKOVSKY
M. MEYYAPPAN
B.J. MORRISON

FEBRUARY 1986

U.S. ARMY RESEARCH OFFICE

CONTRACT: DAAG29-82-C-0023

Prepared by

SCIENTIFIC RESEARCH ASSOCIATES, INC.
P.O. BOX 498
GLASTONBURY, CONNECTICUT 06033

UNCLASSIFIED 28 February 1986

SECURITY CLASSIFICATION OF THIS PAGE (When Data Entered)

ADA 165 464

REPORT DOCUMENTATION PAGE

READ INSTRUCTIONS BEFORE COMPLETING FORM

1. REPORT NUMBER ARO 18480.5-EL	2. GOVT ACCESSION NO. N/A	3. RECIPIENT'S CATALOG NUMBER N/A
4. TITLE (and Subtitle) Transient Transport in Binary and Ternary Semiconductors		5. TYPE OF REPORT & PERIOD COVERED Final Report 27/09/82 - 26/09/85
		6. PERFORMING ORG. REPORT NUMBER
7. AUTHOR(s) H.L. Grubin, J.P. Kreskovsky, M. Meyyappan, B.J. Morrison		8. CONTRACT OR GRANT NUMBER(s) DAAG29-82-C-0023
9. PERFORMING ORGANIZATION NAME AND ADDRESS Scientific Research Associates, Inc. P.O. Box 498 Glastonbury, CT 06033		10. PROGRAM ELEMENT, PROJECT, TASK AREA & WORK UNIT NUMBERS
11. CONTROLLING OFFICE NAME AND ADDRESS U. S. Army Research Office Post Office Box 12211 Research Triangle Park, NC 27709		12. REPORT DATE 27 February 1986
		13. NUMBER OF PAGES 5
14. MONITORING AGENCY NAME & ADDRESS (if different from Controlling Office)		15. SECURITY CLASS. (of this report) Unclassified
		15a. DECLASSIFICATION/DOWNGRADING SCHEDULE

16. DISTRIBUTION STATEMENT (of this Report)

Approved for public release; distribution unlimited.

17. DISTRIBUTION STATEMENT (of the abstract entered in Block 20, if different from Report)

NA

18. SUPPLEMENTARY NOTES

The view, opinions, and/or findings contained in this report are those of the author(s) and should not be construed as an official Department of the Army position, policy, or decision, unless so designated by other documentation.

19. KEY WORDS (Continue on reverse side if necessary and identify by block number)

Nonlinear transport, semiconductors, microelectronics, quantum transport, Boltzmann transport, drift and diffusion, gallium arsenide, aluminum gallium arsenide, indium gallium arsenide, transient transport.

20. ABSTRACT (Continue on reverse side if necessary and identify by block number)

A description of recent studies of two and three terminal band structure dependent compound semiconductors is given.

DD FORM 1 JAN 73 1473 EDITION OF 1 NOV 65 IS OBSOLETE

UNCLASSIFIED 28 February 1986

SECURITY CLASSIFICATION OF THIS PAGE (When Data Entered)

TRANSIENT TRANSPORT IN BINARY AND TERNARY SEMICONDUCTORS

H.L. Grubin, J.P. Kreskovsky, M. Meyyappan and B.J. Morrison
Scientific Research Associates, Inc.
P.O. Box 498
Glastonbury, Connecticut 06033

The objectives of this study were several fold: 1) To examine space and time dependent transport in gallium arsenide, aluminum gallium arsenide, and indium gallium arsenide; 2) To begin a reformulation of quantum transport for mixed states. The technique used for studying transient transport was through solutions to the moments of the Boltzmann transport equation. The quantum transport was primarily formulatory.

In examining the binary and ternary transport application of Vegards rule was applied to determining the effective masses and a variety of other band structure parameters. The parameters for indium arsenide and aluminum arsenide were obtained from previous calculations of Littlejohn, et.al., and modified for implementation using the moments of the Boltzmann transport equation. The initial calculations for steady state were performed using parabolic bands. It became immediately apparent that the parabolic band structure would be inadequate for examining transport. Thus during the initial phases of the study, the moments of the Boltzmann transport equation were modified to include the presence of generic energy versus momentum dispersion relationships. All calculations, however, were performed for the situation in which $\varepsilon + \varepsilon^2/\varepsilon_g = \hbar^2 k^2/2m^*$, where ε_g is the separation between the conduction band minimia and the top of the valence band. Nonparabolicity was used for the Γ, L, and X portions of the conduction band for all semiconductors of interest.

In all calculations a displaced Maxwellian distribution function was used. For the case of parabolic bands, the derived moments of the Boltzmann transport equation are direct and have been published in variety of places including those by the Principal Investigator. A new feature introduced under the ARO study was the implementation of the displaced Maxwellian for nonparabolic bands. In this case, it was necessary to expand the formal displaced Maxwellian, $f(\vec{r},\vec{k},t)$ in powers of k. The expansion as performed in this study consisted of four terms:

$$f(\vec{r},\vec{k},t) = f_0 + f_1 + f_2 + f_3 \qquad (1)$$

higher order terms were ignored. Most, if not all, previous discussions of nonparabolic transport have included only the f_0 and f_1 terms. The departure in this study was the inclusion of the f_2 and f_3 terms. The first question investigated was: How important is the inclusion of the f_2 and f_3 terms?

To determine the importance of the f_2 and f_3 terms, the moments of the Boltzmann transport equation, which had already been obtained exactly for parabolic bands was rederived for **parabolic** bands using the four term expansion. It was determined that the form of the moment equations, as obtained using the complete parabolic displaced Maxwellian, and the four term expansion, were identical only when all four expansion terms were included. This result indicated that all previous nonparabolic studies using the moment equations and only the f_0 and f_1 terms were significantly incomplete. The summary in the next few paragraphs discusses the significance of these latter contributions, as well as the general nonparabolic contributions which have not been discussed in the past.

To begin, it is worthwhile to restate the obvious, particularly, when nonparabolic transport is considered: The transient dynamics of carriers both under uniform and nonuniform field conditions, involves momentum transport rather than velocity transport. The moments of the Boltzmann transport equation describe the time dependence of carrier momentum, and all overshoot phenomena which is generally ascribed to velocity, is rather **momentum overshoot.** Under uniform field conditions, the time rate of change of carriers due to intervalley transfer, is affected only through nonparabolic contributions to the scattering intervals. Under nonuniform field conditions the divergence term, $\mathrm{div}(n\hbar k/m)$, which appears in the continuity equation, is unchanged in form for both parabolic and nonparabolic bands. The significance physics, however, is altered: For parabolic bands $\hbar k/m$ is the mean carrier velocity; for nonparabolic bands it is not.

With regard to momentum balance for uniform fields, the form of the equation is the same for both parabolic and nonparabolic bands. The only alteration is in the nonparabolic contribution to the momentum scattering integrals. However, for nonuniform fields there is a significant alteration in the pressure tensor. The alteration in the pressure tensor for nonparabolic bands arises from the f_2 contribution in the expansion of the distribution function. Complete cancellation of the f_2 contribution occurs for parabolic bands.

With regard to the third moment equation, the equation for energy balance, we find nonparabolic contributions arising even for uniform fields. First it is noted that there are nonparabolic contributions to the energy scattering integrals. Of more significance, it is a fact that the time derivative of the mean thermal energy of the electrons, $\partial[3/2nk_BT_e]/\partial t$, becomes $\partial[3/2nk_BT_eg(T_e)]/\partial t$. The effect in sample calculations of the contribution $g(T_e)$ is to increase the time to relaxation. Under nonuniform field conditions, the kinetic energy contribution undergoes similar alterations. There are additional changes, each of which can be traced to the inclusion of the f_4 term in the expansion of the distribution function. Again, under parabolic conditions, these additional terms undergo specific cancellation. In summary, the presence of nonparabolic band structure significantly alters the form of the governing equations for transient transport within the framework of the moments of the Boltzmann transport equation. The question next is: How do these changes alter our picture of velocity overshoot in semiconductor devices?

The typical way in which transient transport problems are attacked under uniform field conditions is as follows: 1) A set of band structure parameters are established which yield steady state velocity versus field curves that

are compared either to experiment, if available, or other calculations. 2) Once an established set of parameters is obtained, the time dependent calculations are performed. The results of these calculations whether through Monte Carlo procedures, moment procedures, or iterative procedures, all show similar velocity overshoot. The wrinkle in this procedure is as follows: For nonparabolic bands another set of band parameters is chosen from which a mean momentum versus field relationship calculated. From an equation relating velocity to momentum, the resulting steady state velocity versus field is obtained. Now, when the transient calculations are performed, the transients involve the approach of the mean momentum to steady state, from which the velocity transient is obtained. From a practical point of view, it will not surprise anyone that the time to steady state with and without nonparabolic contributions is different. But we are not interested solely in transients to steady state. For example: When a negative differential mobility element is designed to operate as an active device under 94GHz constraints, it is necessary to transfer carriers from the Γ to L and X valleys, and back. One criteria for sustained oscillations is that the peak to valley velocity ratio be sufficiently high. This implies that a significant amount of electron transfer from the Γ valley has occurred. For nonparabolic bands, insofar as velocity and moment are not linearly related, there are situations where a large peak to valley ratio in velocity does not necessarily imply a similarly large peak to valley ratio in momentum. This has emerged from calculations in which the compound semiconductors were placed in a circuit containing reactive elements. Thus a new criteria must be established for determining the upper frequency limit for active device operation in which nonparabolic contributions are introduced. Consider next, the effects associated with nonparabolicity in semiconductors.

Calculations were performed to determine specific nonparabolic effects. These nonparabolic effects were observed for GaAs, InGaAs, and AlGaAs. For example: Steady state calculations were performed for GaAs subject to parabolic bands. The field dependence of velocity, carrier density, and electron temperature for each of the three valleys were obtained. For the same set of band structure parameters, e.g., phonon frequencies, intervalley deformation potential coupling coefficients, etc., the calculation was redone, but with a nonparabolic dispersion relationship. Under steady state conditions, the only alteration in the equations is in the scattering integrals. The results of the calculation were initially, partly unexpected. First, as anticipated the presence of nonparabolic bands reduced the low field mobility of GaAs from its parabolic value. The unusual result was that the alteration in the scattering rates also effected the rate of electron transfer. The result being that more carriers were retained in the Γ valley than were expected from parabolic calculations. There was thus, an apparent 'improvement' in the 'calculated' velocity field curve. There cannot, of course, be any 'improvement' in the velocity field curve, and so the band structure parameters for the GaAs required readjustment to agree with experiment. It is noted that very similar results were reported by A. Sher, at the recent 1986 DARPA EHF Review. These characteristics were also seen for ternary materials.

The above discussion with concerned specifically with the effects of nonparabolic behavior. The InGaAs and AlGaAs studies were performed within the context of broader goals. First, it was anticipated that the band structure of InGaAs was such that a larger fraction of carriers could be retained in the

Γ valley than was possible for GaAs, and that with its high mobility, it would offer superior current drive capabilities for submicron applications than GaAs, but that its inferior high field saturated drift velocity would make it less useful than GaAs. Nonuniform field calculations for submicron GaAs and InGaAs were performed and demonstrate the superior current drive characteristics of the InGaAs. An additional question was asked with respect to GaAs versus InGaAs (note, in this discussion we are concerned with a 50% In concentration); namely, what are the upper frequency limits of GaAs versus InGaAs. Others have addressed this question, and have concluded that the upper frequency limit of GaAs is higher than that of InGaAs. Indeed, a recently completed DARPA study performed by the Principal Investigator, using very general scaling concepts corroborates this result. The final conclusions, however, are not in. For example: Nonuniform field calculations were performed through solutions to the Boltzmann transport equation to simulate Gunn oscillations. These oscillations involve the movement of dipole layers from a nucleation site to a collecting site. Oscillations in GaAs have been measured at frequencies somewhat in excess of 100GHz. Comparative GaAs and InGaAs calculations were performed. Both of them require different levels of background doping to achieve high frequency oscillations. Both semiconductors displayed oscillations in the 100GHz regime. A comparative upper frequency limit has not been obtained yet. Further work is needed. It is noted that in the nonuniform field calculations all transport was assumed to be parabolic.

The situation with AlGaAs was also considered. Here calculations were performed with varying compositions of AlGaAs. The experimental observation of a significant dip in the mobility near a 50% composition of Al was not observed, even when alloy scattering was included. It may be anticipated that such quantities as the deformation potential coupling coefficient will require significant nonlinear increases near this composition range to account for the dip in mobility. Major attention was, however, focused on a 30% composition of Al. Within this range AlGaAs exhibited a marginal region of negative differential mobility. The interest in the AlGaAs is clear from the point of view of the new heterostructure studies, and calculations were performed for AlGaAs/GaAs HEMT devices.

The HEMT studies were performed using the semiconductor drift and diffusion equations and reveal the following results, some of which were initially surprising. The first result was that while a two dimensional electron gas formed at the AlGaAs/GaAs interface, it wasn't as had been expected confined to a narrow, sub-100Å width. Rather, there was significant charge injection within the semi-insulating substrate, and within the heavily doped AlGaAs region. This result was initially quite controversial. And it wasn't until very recently, that we understood the origin of the result to rest with the diffusivity assumption of the calculation. For example: In virtually all HEMT studies, both analytical and numerical, the Einstein relationship has been assumed. This relationship underestimates the high field diffusivity and as our studies indicated, result in narrow confinement. We have used an empirical relationship that more closely represents experimental observation and permits higher diffusivity. This latter result is responsible for the numerical results.

The above discussion involves solutions to both the semiconductor drift and diffusion equations and the moments of the Boltzmann transport equation. As is well known there are difficulties when one is considering transport at

heterostructure interfaces. To overcome these difficulties, we have been directly involved in formulating quantum transport for submicron devices. Initially, in 1981, through application of the Wigner distribution function, a series of moment equations were formulated for pure state. In the absence of scattering, only the first two of those equations were independent. These two equations were equivalent to Schrodinger's equation. During the course of the ARO study, the moment equations were generalized to a mixed state. In generalizing these equations, the formulation was performed in terms of the density matrix rather than the Wigner function, although the two are related through a transformation. In this formulation it was immediately apparent that a separation could be established isolating specific quantum contributions from the classical contributions. Further, it was also immediately apparent that no assumptions on the properties of the potential were necessary, other than the fact that the potential seen by the carriers be continuous.

Each of the above studies: Boltzmann transport, drift and diffusion, and quantum transport have been presented at major technical meetings, summer schools, and government reviews. They are all being prepared for technical publication. Copies of publications arising from this study are included with this report. A list of open presentations is given below.

PRESENTATIONS

Scaling and Band Structure Transport, 1983 APS March Meeting.

Large Signal Numerical Calculations of Three Terminal Selectively Doped Heterostructure Field Effect AlGaAs/GaAs Transistors, 1985 WOCSEMMAD.

Role of Diffusivity in HEMT Calculations, 1986 WOCSEMMAD.

Moments of the Density Matrix Incorporating Dissipation, 1985 Quantum Transport Workshop.

A Study of the Moments of the Density Matrix with Applications to Ultrasubmicron Structures, 1986 APS March Meeting.

A-1

Surface Science 132 (1983) 594-622
North-Holland Publishing Company

THE ROLE OF BOUNDARIES ON HIGH SPEED COMPOUND SEMICONDUCTOR DEVICES

H.L. GRUBIN and J.P. KRESKOVSKY

Scientific Research Associates, Inc., P.O. Box 498, Glastonbury, Connecticut 06033, USA

Received 2 September 1982; accepted for publication 11 November 1982

The role of boundaries and interfaces on the electrical characteristics of long and submicron scale compound semiconductor devices is discussed.

1. Introduction

Theoretical and experimental studies of compound semiconductor devices over the past decade have demonstrated that conditions at the device boundaries are the most important determinant of the operating characteristics of the device. Studies in long two-terminal gallium arsenide devices [1], indium phosphide [2], germanium [3], and cadmium sulphide [4] have demonstrated that conditions at or near the contacts control the current–voltage relations and the electrical characteristics of any resulting instabilities. For two-terminal devices it is often possible to correlate the pre- and post-threshold device behavior. For three-terminal devices, most interface studies have focused on the role of the layer just under the principle region of electron transport. In the case of gallium arsenide field effect transistors, heterostructure interfaces have been incorporated with the object, e.g., of confining carriers to the active region in the case of a heavily doped active region, [5,6], or of providing a sea of carriers in a nominally undoped region.

In near and submicron scale devices, the relative importance of the boundaries increases as these regions occupy a sizeable fraction of the device active region length, and the up- and downstream boundaries begin to communicate with each other. Controlling these boundaries is likely to be the most significant task of device physics studies in the immediate future. The motivation for this outlook is based upon the fact that transport on a near and submicron scale involves nonequilibrium effects on a picosecond time frame, and its effectiveness is based on transport by high mobility carriers. Thus, questions such as: "How many carriers are injected into the Γ valley of gallium arsenide, and with what energy and velocity?" enter the picture prominantly.

0039-6028/83/0000-0000/$03.00 © 1983 North-Holland

The purpose of this paper is to highlight the effects of boundaries on compound semiconductor devices, particularly gallium arsenide. In doing so, the discussion is separated into two parts: (1) the role of boundaries on long, low frequency (< 20 GHz) gallium arsenide devices, and (2) the role of the boundary on high frequency near and submicron scale devices.

For long devices in which a rich body of experimental work exists, a review of boundary effects is given in terms of a "pinned" cathode field and "pinned" cathode current model. The basis for these models is the notion that contact boundaries may be *phenomenologically* represented as either tunneling or thermionic emission dominated regions, with a varying barrier height. The description of long devices assumes that all picosecond scale transients have occurred, and that all band structure population statistics are adquately represented by steady state conditions.

For the shorter devices it is the short time transients and the spatial and temporal transients within the bands that are calculated. The description requires solutions of the Boltzmann transport equation and resolution on the scale of a fraction of a bulk mean free path is needed. These problems are discussed in section 3 where a review of such phenomena as velocity overshoot is given. The ability to attain contact and boundary effects permitting the realization of the high overshoot speeds in devices is the core on which the studies of section 3 are based.

All of the theoretical studies presented arise from solutions of differential equations. For long devices,the "drift and diffusion" equations are solved. For short devices, moments of the Boltzmann transport equation are solved. In both cases true contacts are represented as boundary conditions to the differential equations. Thus, the studies illustrate the *effects* of the contacts and/or interfaces on device behavior. The results of these studies, when successful, tend to highlight what is unknown about device material parameters. For the case of long devices, it is the cathode boundary condition that is unknown. Here the sensitivity of the results to varying the cathode field identifies the significance of the contacts on device behavior [1]. Similar sensitivity studies are discussed in connection with solutions of the Boltzmann transport equation, where a range of parameters is chosen to identify the conditions for "injecting" and "blocking" contacts. A sensitivity analysis of the electronic contribution to the thermal conductivity is also included as its effects are dramatic.

2. Boundary conditions to negative differential conductivity devices

In this section a brief review of the influence of boundaries on the behavior of NDC devices is given. Fig. 1 displays typical boundary-dependent data from three different gallium arsenide two-terminal devices [7]. The lower portion of

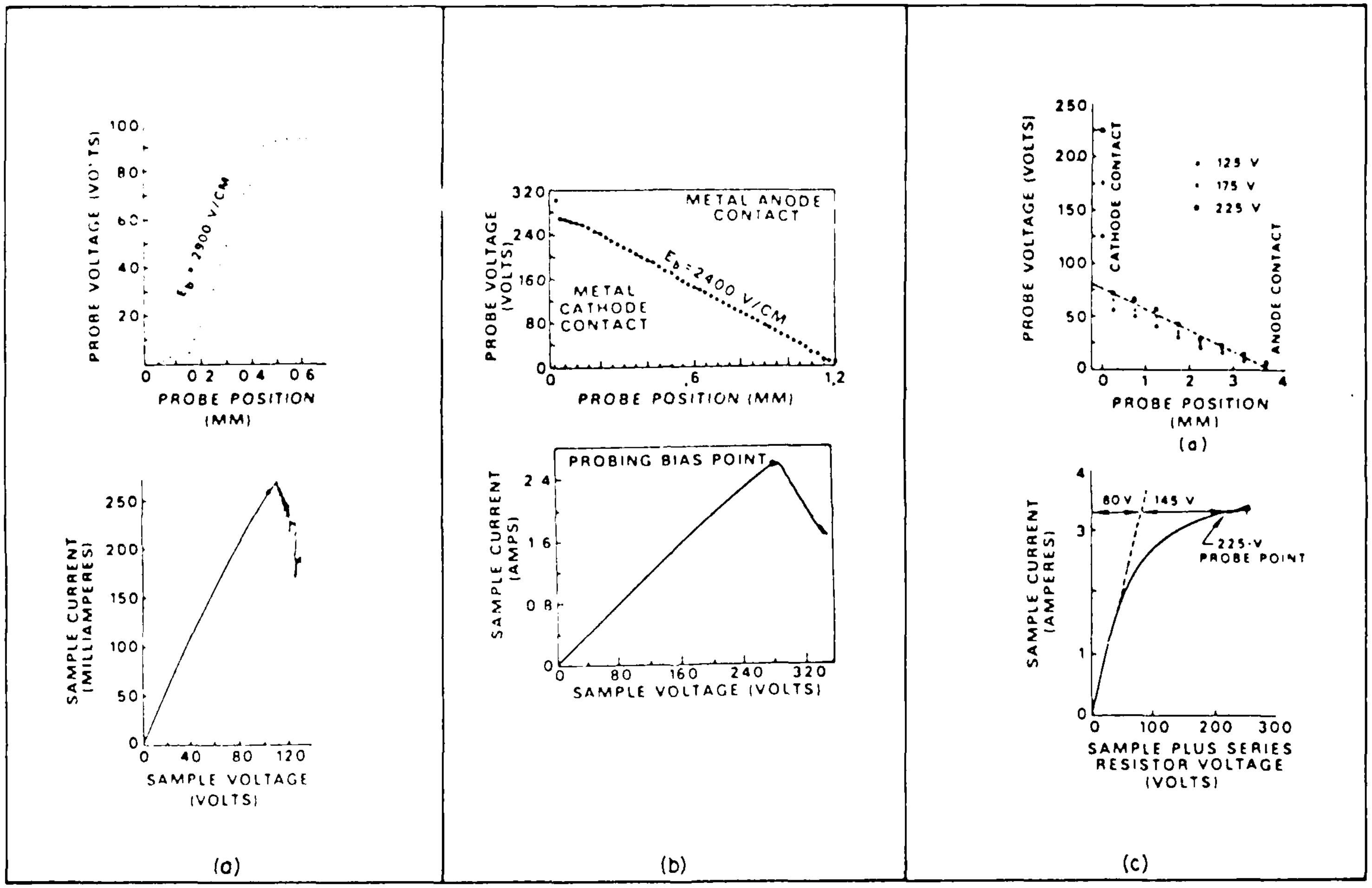

Fig. 1. (a) Current versus voltage for a low cathode field GaAs sample with a conductivity mobility of 5900 $cm^2/V \cdot s$. Sample was sculptured into an "H" shape to remove active region from boundaries. Also shown is the probed voltage versus distance. Probing bias is indicated by closed circle. (b) As in (a) but for an intermediate cathode field. Sample was "parallelepiped" shaped without any deliberate shaping. (c) As in (b) but for a high cathode field sample. From ref. [7] with permission.

each diagram displays current versus voltage characteristics, while the upper portion shows voltage versus distance at one bias point. Fig. 1a shows measurements for a device in which the metal contacts are far removed from the active region of the device. The current–voltage relation is relatively linear until a point where current oscillations occur. The field profile just prior to the oscillation is relatively uniform within the active region of the device, and is near zero at the ends of the active region. Fig. 1b represents a set of measurements in which the metal contact abutted the active region of the device. The current–voltage characteristics remained linear to threshold which again was manifested by a current oscillation. Notably different here is the lower average field prior to the instability and the enhanced voltage drop at the cathode. Fig. 1c displays results for another device with a metal contact abutting the active region. For this case there is a sublinear current voltage characteristic and no instability. The probed voltage versus distance shows a large voltage drop at the vicinity of the cathode.

The electrical characteristics associated with fig. 1 have been described as representative of "ohmic" (fig. 1a), "slightly blocking" (fig. 1b), and "strongly blocking" (fig. 1c) contacts. One of the earliest models employed for explaining these results assumed a "pinned" value of cathode electric field [1]. Other models in which the cathode conductivity [8] or doping [9] have also been suggested with varying degrees of success. The "pinned" cathode field model developed, partially as a consequence of the way the governing equations describing current instabilities was written. Here the one-dimensional differential equation for total current,

$$J(T) = q\left(NV - D\frac{\partial N}{\partial X}\right) + \epsilon\frac{\partial E}{\partial T}, \tag{1}$$

was rewritten, using Poisson's equation, as

$$J(T) = qN_0V + \epsilon\left(V\frac{\partial E}{\partial X} - D\frac{\partial^2 E}{\partial X^2} + \frac{\partial E}{\partial T}\right). \tag{2}$$

This is a second order partial differential equation requiring two boundary conditions on $E(X, T)$ and one initial condition. In the above $J(T)$ represents current density, N is carrier density, V and D are field dependent velocity and diffusion.

Solutions to eq. (2) have been used successfully to simulate device results similar to those of fig. 1. For gallium arsenide in which the threshold field for negative differential mobility is approximately 3.2 kV/cm = E_{TH}, qualitatively similar results occur for solutions with cathode fields falling into any one of the following three groups: $0 \leq E(X=0, T) \leq E_{TH}$, $E_{TH} \leq E(X=0, T) < 4\,E_{TH}$, $E(X=0, T) > 4\,E_{TH}$. The simulations with pinned fields falling in either group 1, 2 or 3 yield electrical characteristics similar to those of figs. 1a, 1b and 1c, respectively. The crucial feature of this model is that the cathode field is

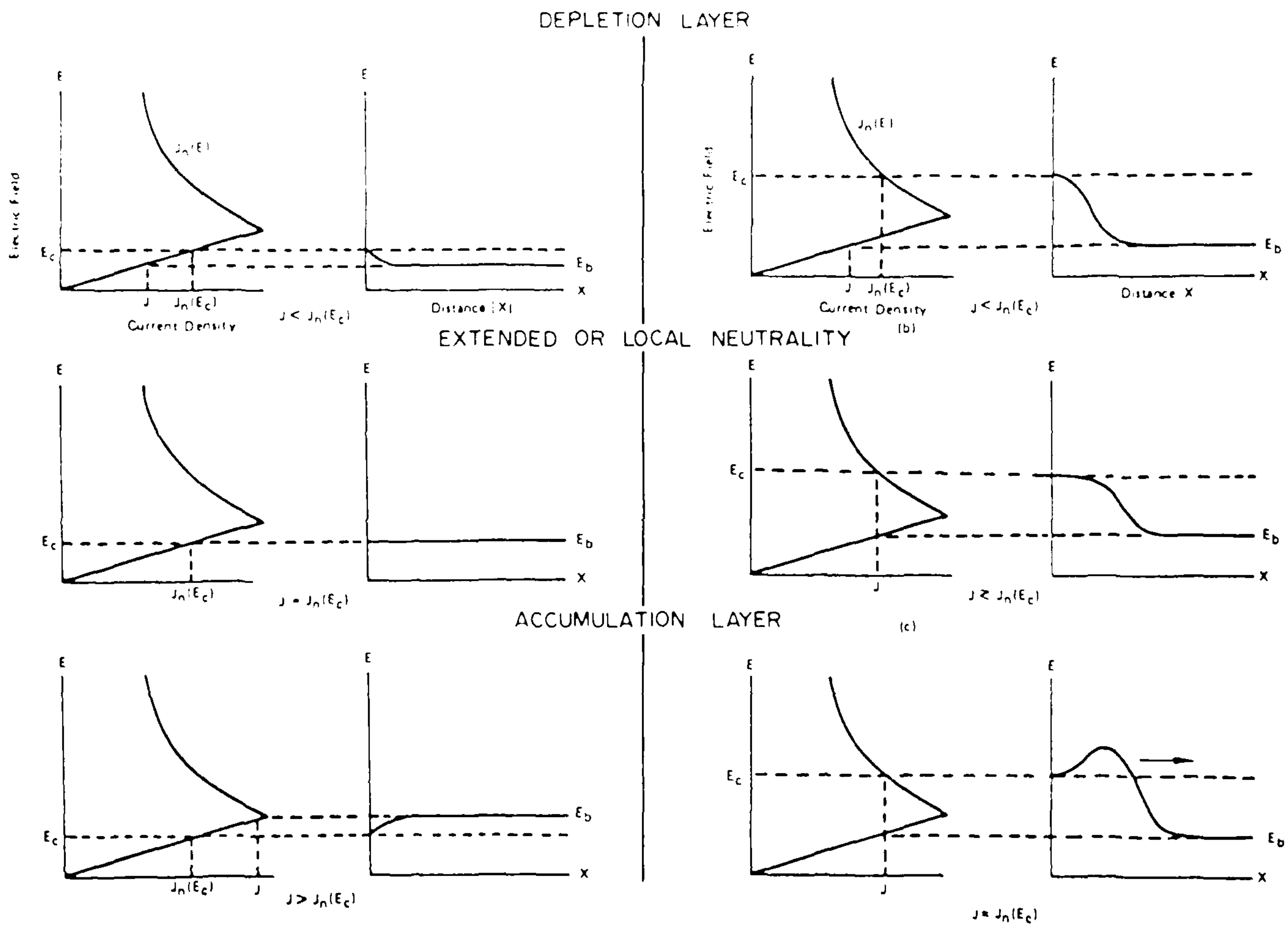

Fig. 2. (a) Electric field versus neutral current density, and electric field versus distance for a pinned cathode field, E_c, within the "ohmic" portion of the velocity field relation. (b) As in (a) but for a pinned cathode field within the NDM region. Curves show trends for cathode depletion, charge neutral, and cathode accumulation. From ref. [10], with permission.

pinned, necessitating that any instabilities in current occur at a critical value of current density. The field profiles associated with cathode fields in the range $0 \leqslant E(X=0, T) \leqslant E_{TH}$, and $E_{TH} \leqslant E(X=0, T) < 4\ E_{TH}$ are sketched in figs. 2a and 2b respectively. For reference, a velocity field curve with velocity scaled to current as $qN_0V(E) = J_n(E)$, and with a region of negative differential mobility is also included. Fig. 2 is understood as follows: The second column of each section shows the electric field versus distance profiles. $E(X)$ begins with a value E_c at the cathode and extends downstream to a value E_b. By current continuity, the current everywhere within the device is given by $J = qNV(E_b)$. For $J < J_n(E_c)$, a region of charge depletion forms near the cathode for E_c below and within the region of negative differential mobility (NDM). Increasing the current until $J \equiv J_n(E_c)$ introduces charge neutrality everywhere for $E_c < E_{TH}$. However, because E is a double valued function of V, for E_c within the NDM region, approximate charge neutrality exists near the cathode for $J \leqslant J_n(E_c)$, and for regions sufficiently far downstream from the cathode. Charge neutrality breaks down between these two regions. Finally, for $J > J_n(E_c)$ an accumulation layer forms near the cathode. For fig. 2a, the accumulation layer is stable until the bulk field exceeds E_{TH}. For fig. 2b, the accumulation layer, followed downstream by the depletion layer, is often unstable and leads to cathode originated instabilities [10].

The situation corresponding to fig. 1c is often represented by very high cathode fields. The field profiles are those appropriate to a wide region of charge depletion near the cathode. The profiles are electrically stable.

The characteristic feature of these nonuniform field profiles is that their structure is significantly affected by the field being a double valued function of velocity. The pinning of the cathode field is not necessarily common, however, to all semiconductor devices. For example, it was also applied to InP devices, where it worked for a significant number of cases. However, a broad class of device behavior could not be accounted for through its use [2]. These devices showed anomalously high efficiency and significantly low DC current levels. Spontaneous Gunn type oscillations did not occur. Rather, device operation required a tuned circuit. The details of the oscillation were thought to depend critically on the cathode boundary condition, which in this case was taken as a fixed cathode conduction current [10,11].

The distinction between "pinned" cathode field and "pinned" cathode conduction current is placed in perspective in fig. 3 and in the following equation

$$J(T) = J_c(E_c) + \epsilon \frac{\mathrm{d}E_c}{\mathrm{d}T}. \tag{3}$$

Eq. (3) is the equation for total current through the boundary to the device. $J_c(E_c)$ represents the current–field relation at the cathode [12] which may be expected to differ from that of the semiconductor device. Two such types of

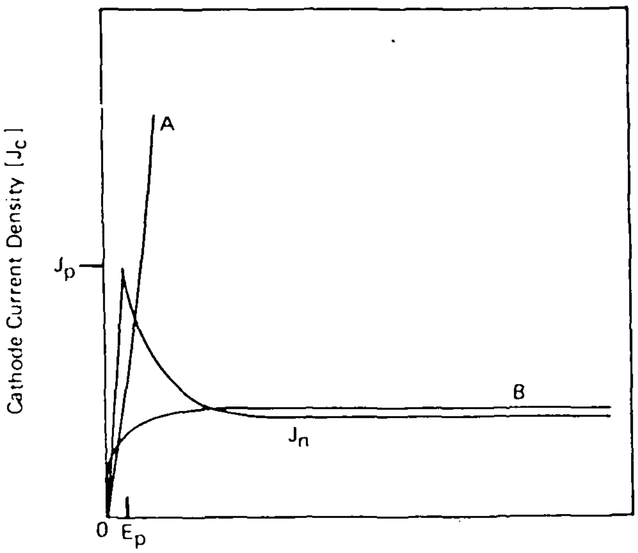

Fig. 3. Cathode conduction current curve for an approximately "pinned" cathode field, curve A; and pinned cathode conduction current (at high field fields), curve B. Curves are obtained from eq. (4). Also shown, for reference, is the neutral current versus field curve for GaAs. From ref. [10], with permission.

curves are represented by curve A and curve B of fig. 3. Curve A is closely related to the pinned cathode field model while curve B is associated with the pinned cathode current model. The similarity in "form" of curves A and B to moderate barrier height tunneling and thermionic emission dominated contacts is deliberate [10], and the equation used to arrive at these curves is shown below

$$J_c(E_c) = -J_R\left\{\exp\left(-\frac{qE_cL_c}{nk\tau}\right) - \exp\left[-\left(\frac{1}{n}-1\right)\frac{qE_cL_c}{k\tau}\right]\right\}, \tag{4}$$

which was adapted from studies on the unalloyed metal/semiconductor contact [13]. Its use here presumes a similar description. For the unalloyed contact, n is the ideality factor and describes the contact as dominated by thermionic emission ($n = 1$) or by tunneling ($n \gg 1$). J_R is the reverse current flux and may be related to the barrier height phenomenologically through the Richardson equation [10].

Detecting a particular contact effect on a device is a difficult procedure. For long devices current voltage characteristics as represented by fig. 1 are often signatures of a contact classification. For short devices proximity effects introduce an additional complication and current–voltage measurements are less valuable. One type of measurement which may serve to provide information about the boundary is a noise measurement.

Here the situation to envision is that if the field is pinned within the

negative differential mobility region, increasing the bias will result in an increase in the length of the NDM region. Any fluctuation will sustain enhanced amplification and the noise will increase. If increasing the bias resulted in carrier injection into the device, the field at the cathode is likely to decrease with increasing bias and the noise is expected to decrease. While these results should be folded in with the field dependence of velocity and diffusion, a simple analytical noise calculation assuming a three piece linear approximation to represent GaAs has been performed [14].

In this calculation, the "impedance field method" [15] is applied to calculating noise due to thermal velocity fluctuations amplified within the device. The mean squared noise voltage per unit band width [15] is computed,

$$\left\langle \frac{\delta V_N^2}{\Delta f} \right\rangle = 4q^2 \int_{\text{vol}} |\nabla Z|^2 \, ND \, \mathrm{d(vol)}, \tag{5}$$

where ∇Z is the impedance field vector [15]. The calculation is performed for a 10 μm long element with a doping of $10^{15}/\text{cm}^3$. The element sustains the field profile of fig. 2b where it is seen that the NDM region increases with increasing bias. The calculations, which are discussed in detail elsewhere, [14] are expressed in terms of the noise figure [16]:

$$\mathrm{NF} = 1 + \left\langle \frac{\delta V_N^2}{\Delta f} \right\rangle \frac{1}{4k_0\tau|R|}, \tag{6}$$

where R is the real part of the device impedance. The results of the calculation are displayed in fig. 4, where the noise figure is sketched as a function of bias current and transit angle. The results appear as a signature of the effects of the cathode boundary. First, at low values of transit angle $\theta = \omega T(\Delta)$, where $T(\Delta)$ is the transit time across the negative differential mobility region, the noise figure increases with increasing bias. This corresponds to an increase in the length of the negative differential mobility region and enhances amplification of any fluctuation originating there. More interesting structure is present at higher frequencies and higher bias where the noise figure increases and then shows a singularity. On the other side of the singularity there is a "U"-shaped region ending again at a singularity. The strong increase in noise figure represents the approach of $|R| \Rightarrow 0$. Here, at low frequencies, the real part of the impedance is positive, and becomes negative at frequencies somewhere between $\pi \leq \theta \leq 2\pi$. In going from positive to negative values it passes through zero, hence the singularity. The frequency range for small signal negative resistance increases with increasing bias [10] reflecting the broadening of the negative differential mobility regions – a broad "U"-shaped region appears. Both the increasing noise figure at low frequencies, and the "U"-shaped region at high frequencies are characteristics of an increasing depletion layer width. Note that increasing the bias still further will result in an electrical instability [10].

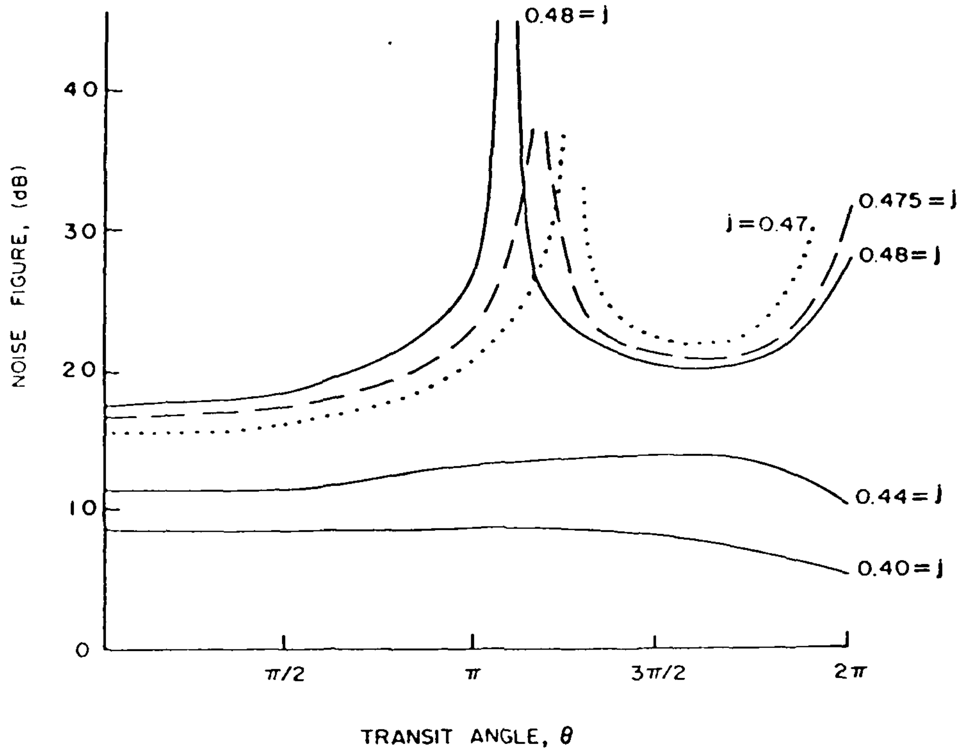

Fig. 4. Noise figure versus transit angle and normalized bias current $j = J_b/N_0eV_p$, for a 10 μm long element with a depletion layer profile. From ref. [14], with permission.

3. Electron transport in near and submicron devices: the role of the boundaries

The discussion of the above sections dealt with devices whose lengths were typically 10 μm long or longer. Transport for these devices is generally discussed though use of the drift and diffusion equation (eq. (1)). For near and submicron length devices electron transfer is generally not complete until a substantial fraction of the device has been traversed. Consequently the drift and diffusion description is inadequate and solutions to the Boltzmann transport equation are required.

For two level transfer in GaAs the steady state velocity field curve for carriers in the central and satellite valleys are shown in fig. 5, where the net velocity V is

$$V = N_1V_1 + N_2V_2. \tag{7}$$

Here the subscript 1 denotes transport in the central valley (Γ valley for GaAs) and the subscript 2 denotes transport in the satellite valley. Most device design is concerned with controlling the time spent by the numbers of carriers in

in valleys 1 or 2; and circuits, interfaces or contacts are sought which will allow for this control. Solutions to the Boltzmann transport equation which provide the required nonequilibrium transport behavior are obtained by a number of

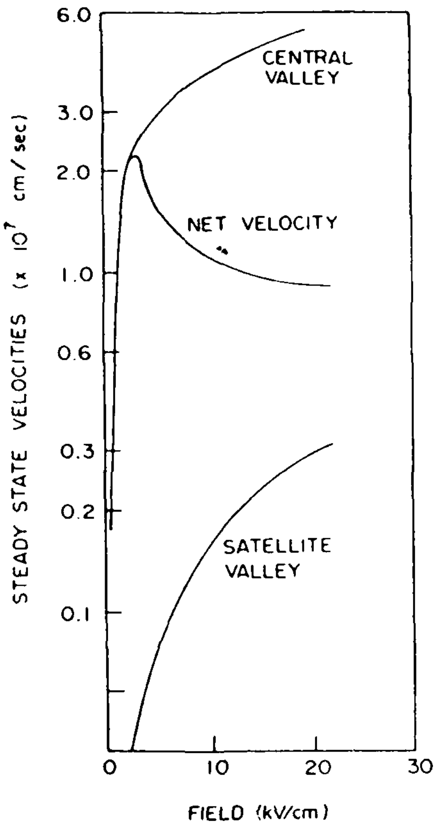

Fig. 5. Steady state velocity versus field curves for Γ and satellite valleys for gallium arsenide. From ref. [22], with permission.

different techniques, the most familiar of which is the Monte Carlo method [17]. Other methods include the Rees iterative technique [18] and balance equation solutions [19], which are considered below.

The balance equations discussed below are the first three moments of the Boltzmann transport equation. They form a subset of the infinite hierarchy of moment equations, and as such do not form a closed set of equations. Each equation introduces a higher order moment not defined by the given set of equations. The most common form of the balance equations is obtained by assuming a distribution function of the form

$$f = f_{0i} \propto \frac{N_i}{\tau_i^{3/2}} \exp\left[-\frac{m(U - V_i)^2}{2k_0\tau_i} \right]. \tag{8}$$

for each species i. More generally [20]

$$f_i = \left(1 + A_k \frac{\partial}{\partial U_k} + A_{kl} \frac{\partial^2}{\partial U_k\, \partial U_l} + A_{klm} \frac{\partial^3}{\partial U_k\, \partial U_l\, \partial U_m} + \dots \right) f_{0i}, \tag{9}$$

where it is insisted that the first term in the expansion gives the correct local values of density, velocity and energy. The coefficients in the above expansion are inversely proportional to density and are model dependent. The first correction to the local equilibrium balance equtions, the so-called hydrodynamic approximation yields

$$\frac{\partial N}{\partial T} + \nabla \cdot (V_i N_i) = \left(\frac{\partial N_i}{\partial T}\right)_c, \tag{10}$$

$$\underline{\frac{\partial \boldsymbol{P}_i}{\partial t} + \nabla \cdot (\boldsymbol{V}_i \boldsymbol{P}_i)} = -eN_i \boldsymbol{F} - \operatorname{grad} N_i k_0 \tau_i - \boxed{\operatorname{div} \boldsymbol{\sigma}'} + \left(\frac{\partial P_i}{\partial T}\right)_{\text{coll}}, \tag{11}$$

$$\frac{\partial}{\partial t} W_i + \nabla \cdot V_i W_i = -eN_i \boldsymbol{F} \cdot \boldsymbol{V}_i - \nabla \cdot \boldsymbol{V}_i N_i k \tau_i - \boxed{\operatorname{div} \boldsymbol{\sigma}' \times \boldsymbol{V}_i}$$
$$+ \boxed{\operatorname{div}(\kappa \operatorname{grad} \tau_i)} + \left(\frac{\partial W_i}{\partial T}\right)_{\text{coll}}, \tag{12}$$

where τ_i is an electron temperature,

$$\boldsymbol{P}_i = N_i m_i \boldsymbol{V}_i, \quad W_i = N_i\left[\tfrac{1}{2} m_i V_i^2 + \tfrac{3}{2} N_i k \tau_i\right],$$

$\boldsymbol{\sigma}$ is a stress tensor arising from nonuniform velocity distributions, and κ is the thermal conductivity. The stress term is dissipative in that when a nonuniform velocity distribution is impressed on an electron stream, there will be reactive forces tending to smooth them out. At this point, however, these terms are regarded as phenomenological entries.

The boxed terms above represent contributions from the nonspherical nature of the distribution function. These contributions have not been included in evaluating the collision integrals, i.e., $(\dots)_{\text{coll}}$ but will be discussed in a future paper. The collision integrals are discussed in ref. [21]. The underlined and boxed terms are ignored in the drift and diffusion approximation.

Under uniform field conditions the mean response of carriers to a sudden change in electric field is shown in fig. 6. The high peak velocity is a consequence of carriers being retained in the Γ valleys for time duration upwards of 0.2 ps before undergoing transfer to the upper valleys. The peak velocity in fig. 6 is extremely high. It represents an upper bound on the carrier velocity that may be expected at this field and provides the motivation for designing boundaries that permit achievement of these values.

The peak velocity, however, is sensitive to bias rise time and hints at problems to be addressed in designing appropriate device boundary conditions. See fig. 7. Furthermore, because a finite time is required for carriers to

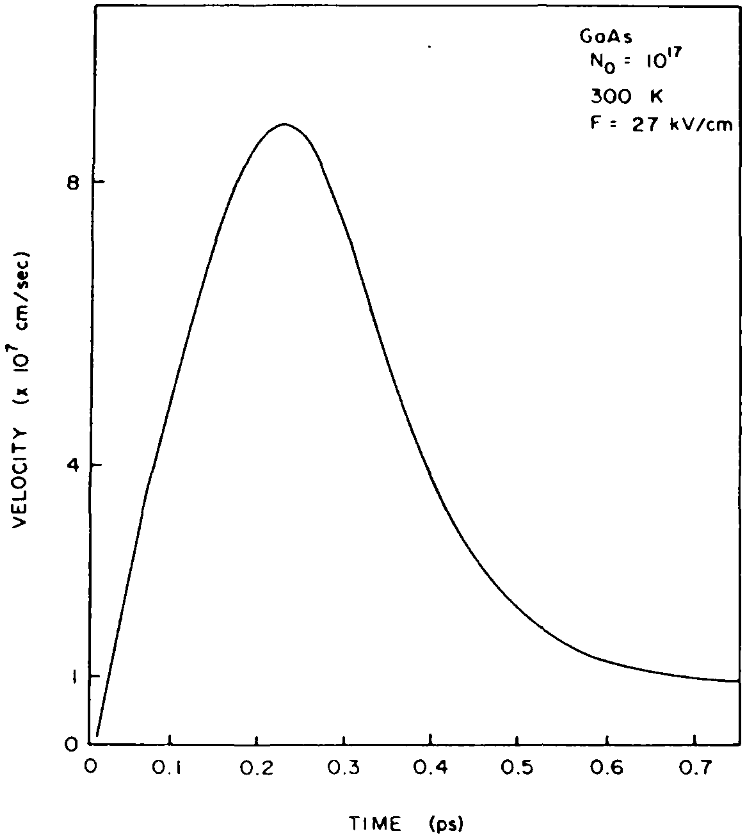

Fig. 6. Transient velocity versus time, for electrons subject to a sudden change in field of magnitude 27 kV/cm. From ref. [22], with permission.

transfer into subsidiary portions of the conduction band, on a near and submicron scale, the velocity field characteristics are expected to be length dependent. See fig. 8. Thus, near and submicron devices will categorically be sensitive to both boundary effects and device length, neither of which will be independent of the other.

Figs. 5 to 8 are signatures of high speed submicron transport. What are the consequences for device behavior? Can a suitable set of contact or interface conditions be found to achieve high speeds associated with overshoot? While a detailed study on a scale similar to that for long devices is not yet available, some results are known. We discuss these below for a collection of 2 μm long devices, essentially undoped, $N_0 = 5 \times 10^{15}/\mathrm{cm}^3$, each subjected to a bias of 2 V. These one-dimensional studies are in steady state, i.e., $\partial/\partial T = 0$, and are subjected to the following cathode boundary conditions:

$$\frac{\partial}{\partial X} \log N_1 = -A, \tag{13}$$

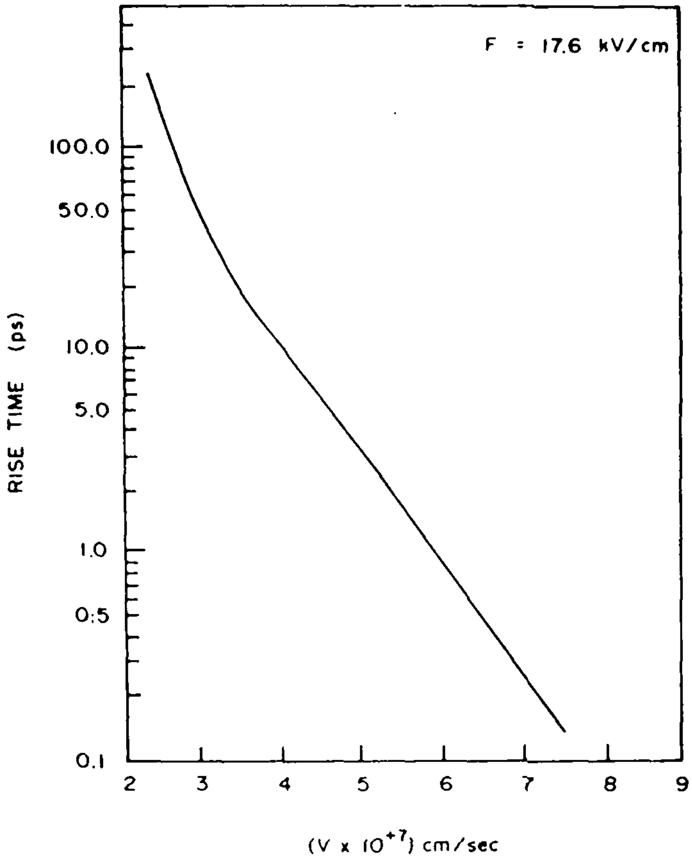

Fig. 7. Peak carrier velocity versus bias rise time for electrons subject to a final field of 17.6 kV/cm.

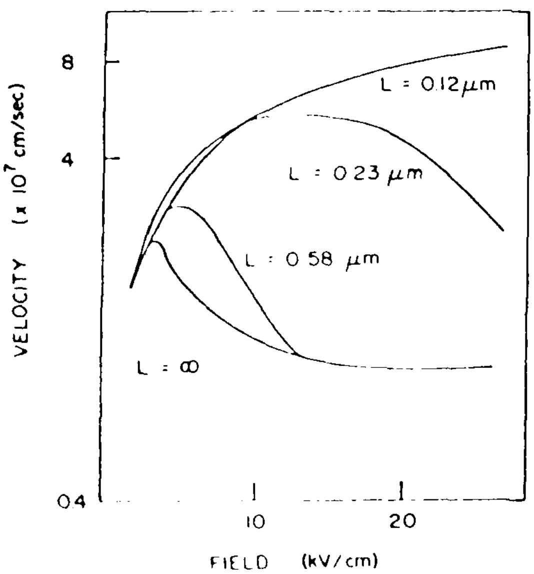

Fig. 8. Exit velocity of carriers at the terminus of a device of specified length, and indicated value of electric field. Carriers enter with zero velocity and are subject to a sudden change in field. From ref. [23], with permission.

$$V_1 = -\mu_c F, \tag{14}$$

$$\tau_1 = B, \tag{15}$$

$$\partial N_2/\partial X = \partial V_2/\partial X = \partial \tau_2/\partial X = 0. \tag{16}$$

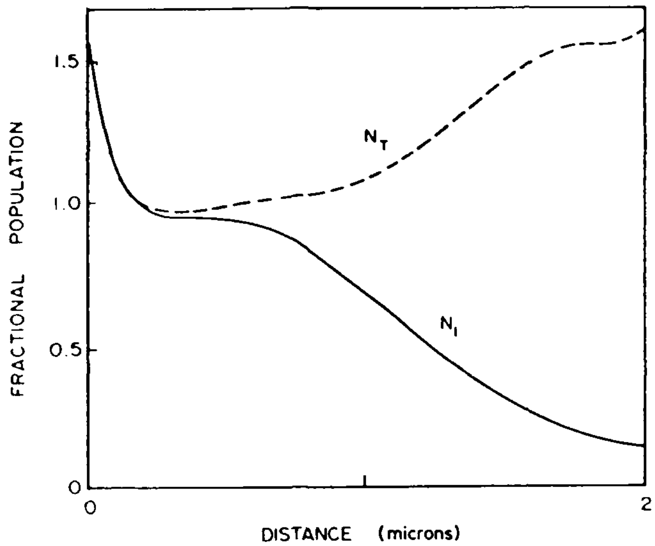

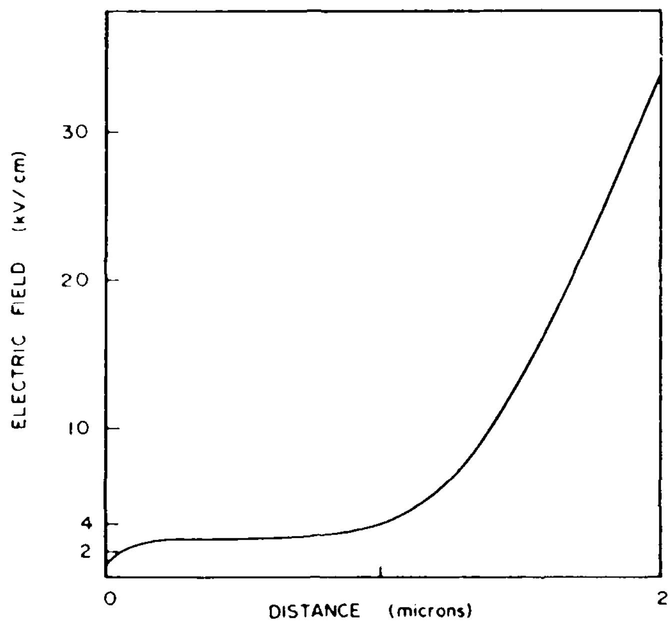

Fig. 9. (a) Fractional population of carriers, N/N_0 in a 2 μm long device with a uniform nominal doping of $5\times10^{15}/\mathrm{cm}^3$, subject to a bias of 2 V. N_T is the total carrier density. N_1 is the carrier density in the central valley. (b) Electric field versus distance. For this calculation $\mu = 12{,}000$ $\mathrm{cm}^2/\mathrm{V\cdot s}$, $A = 0.2$ and $B = 300$.

For A positive (negative) local charge accumulation (depletion) occurs at the cathode boundary. B is generally greater than, or equal to, 300 K and is a measure of the mean thermal energy of the Γ-valley carriers. As in section 2, the results are placed into three categories, "ohmic", "slightly" and "strongly" blocking contacts. The "ohmic" results are shown in fig. 9.

For "ohmic" boundaries an appropriate set of constants, with ref. [19], are: $A = 0.2$, $\mu_c = 12{,}000$ cm^2/V · s, and $\tau_1 = 300$. For this case carriers enter the device with speeds greater than that associated with the central valley mobility. Consequently there is an accumulation of carriers at the boundaries, resulting in low values of cathode field. The field starts off at nearly 1 kV/cm and approximately 2500 Å must be traversed before significant transfer occurs. Increased transfer results in a lowering of the mean carrier velocity, necessitating an increase in mobile charge as the anode is approached. The average velocity across this device obtained from the relation

$$V_{av} = J/qN_0 \tag{17}$$

is $V_{av} = 1.78 \times 10^7$ cm/s, with $N_0 = 5 \times 10^{15}$/cm^3. The advantage of overshoot is not fulfilled by this contact device length configuration.

Lowering the cathode mobility to a value below that associated with the Γ valley results in a more rapid dispersal of carriers, and cathode adjacent charge depletion, associated with slightly blocking contacts, occurs. This is seen in fig. 10 for $A = -0.11$, $\mu_c = 6000$ cm^2/V · s, and $\tau_1 = 300$ K. It is noticed that the cathode field for this case is approximately 4 kV/cm, which is higher than that associated with the "ohmic" contact condition of fig. There are, however, important similarities between figs. 9 and 10. In both cases the carriers adjacent to the cathode are, for all practical cases, Γ-valley electrons. Very little transfer, which is determined by carrier energy (temperature), has occurred. In addition, sufficiently downstream from the cathode the carriers appear to be ignoring the cathode condition and are dominated by the downstream voltage drop, whose spatial distribution is about the same for both. The average velocity for this case is $V_{av} = 1.75 \times 10^7$ cm/s, slightly below that of fig. 9.

A significant change occurs when the mean energy of the Γ-valley entering carriers is elevated. For the parameters of fig. 10, but with $\tau_1 = 1200$ K, a substantial amount of transfer occurs at the cathode, resulting in a lowering of the current through the device. The cathode field is approximately 7 kV/cm, higher than that associated with fig. 10, and the downstream field is lower (see fig. 11). The average velocity of the carriers in this case is lowered to 1.28×10^7 cm/s, even though the central valley carriers are traveling at higher speeds (see fig. 5).

The presence of moderately high cathode fields is attractive if a sufficient number of carriers can be retained in the central valley where they can sustain high transit velocities. While this case is discussed in more detail below, the simple ruse of injecting excess carriers into a device with the contact conditions

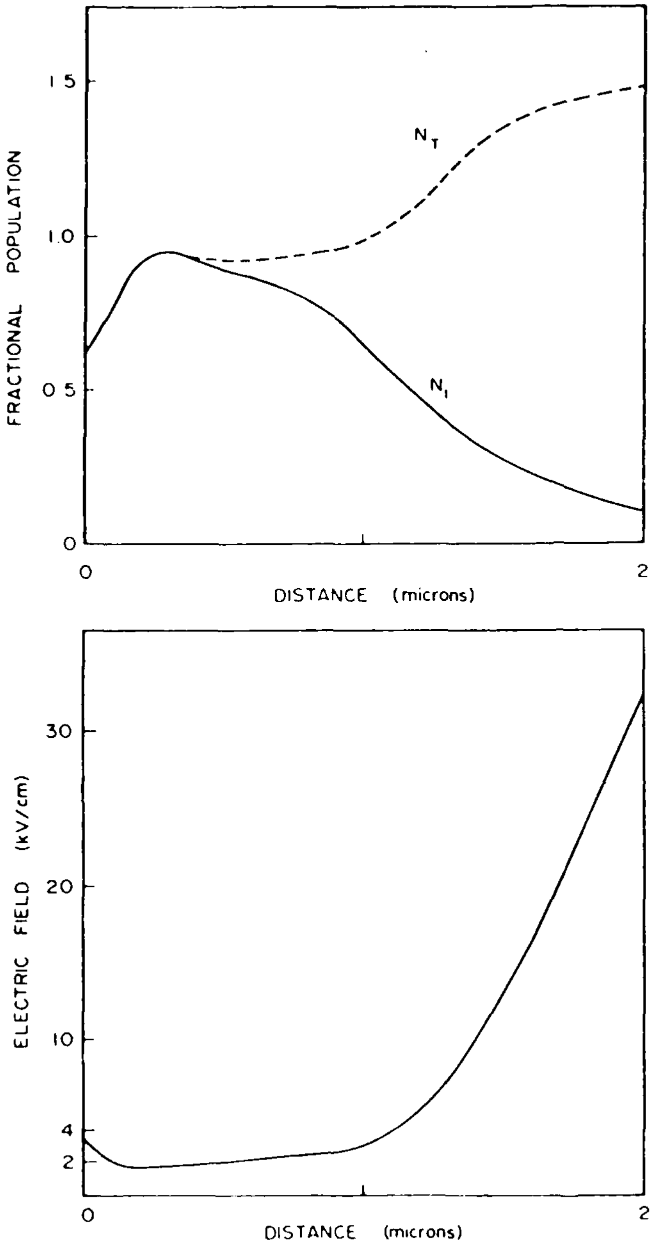

Fig. 10. As in fig. 9, but with μ_c = 6000 cm^2/V·s, $A = -0.11$ and B = 300 K.

of fig. 11 does not always yield the sought after current levels. This is illustrated in fig. 12, where now $A = 0.2$. Here, the excess charge serves to lower the cathode field, which does not change the downstream characteristics in any significant way. The average velocity for this case is virtually unchanged

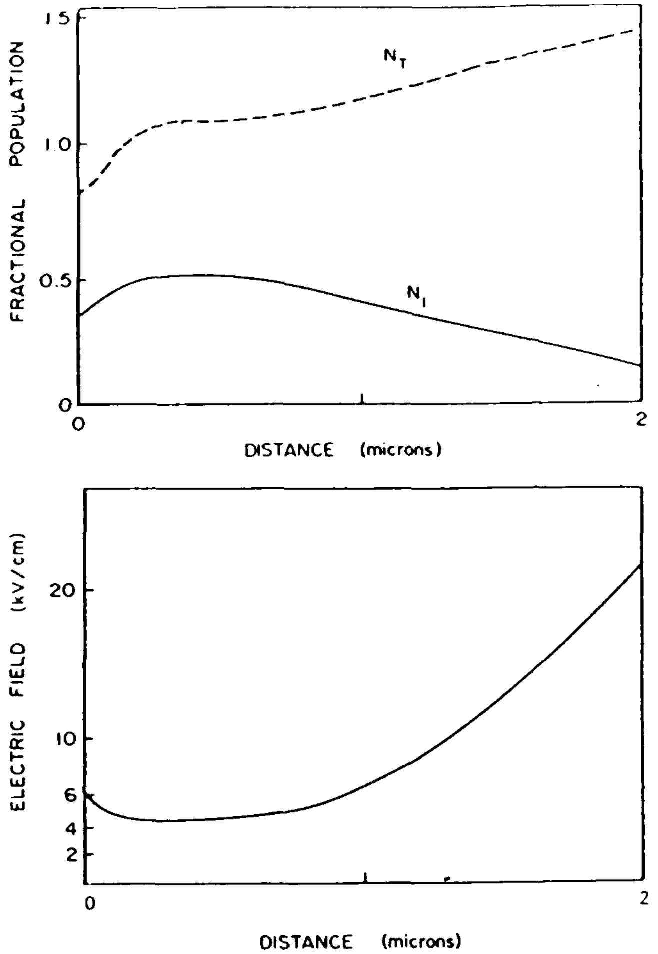

Fig. 11. As in fig. 9, but with $\mu_c = 6000$ cm^2/V·s, $A = -0.11$ and $B = 1200$ K.

when compared to fig. 11. In this case $V_{av} = 1.30 \times 10^7$ cm/s.

The situation of a strongly blocking contact is illustrated in fig. 13 for $A = 9.0$, $\mu = 1000$ cm^2/V · s, and $T = 3000$ K. For this case virtually all carriers are swept away from the cathode, with the satellite valley carriers accounting for most of the transport in the transition region. The cathode field is extremely high, approaching 60 kV/cm. The average velocity is approximately zero.

The above results focus attention on the role of the upstream boundary in the distribution of charge near the interface. The results are more general than those obtained using the steady state field dependent velocity relation, especially in identifying the fact that electron transfer, *even in the case of partially blocking contacts*, may not occur until some point downstream from the

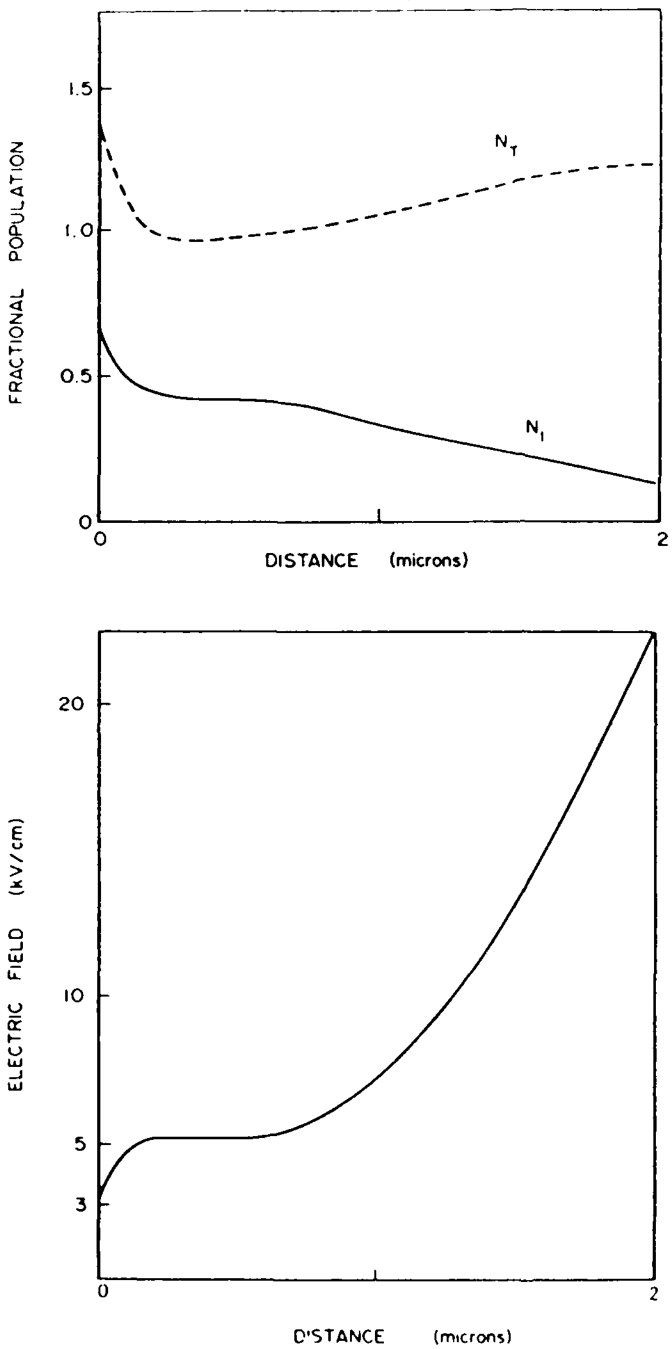

Fig. 12. As in fig. 9, but with $\mu_c = 6000$ cm^2/V·s, $A = 0.2$ and $B = 1200$ K.

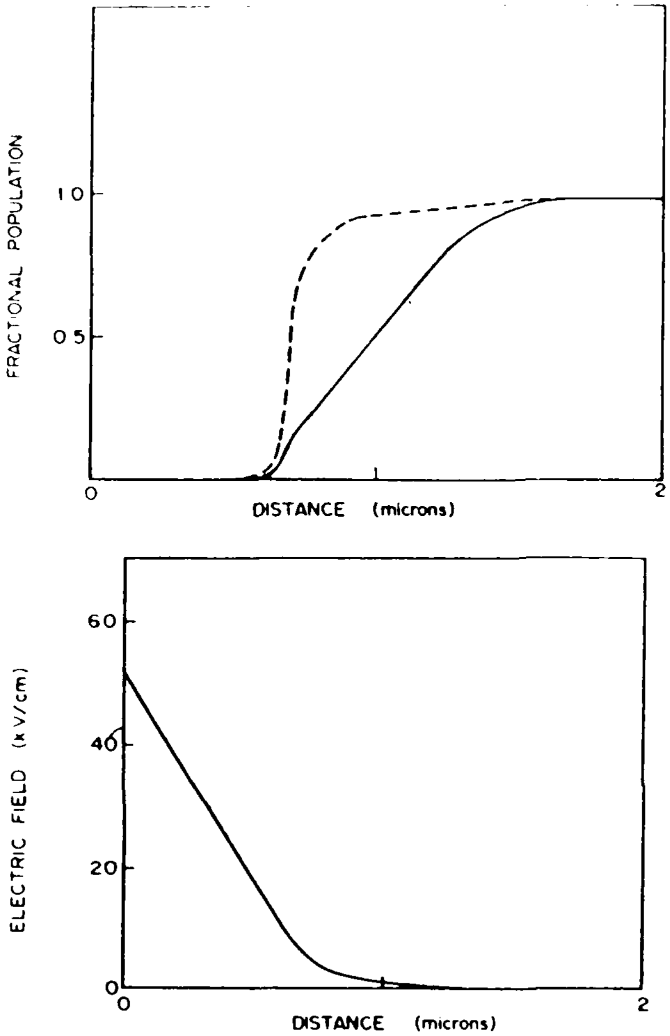

Fig. 13. As in fig. 9, but with $\mu_c = 1000\ cm^2/V \cdot s$, $A = -9.0$ and $B = 3000$ K.

cathode contact. The implication of this is that the detailed role of the contact in controlling current instabilities may need generalization. On another matter, it is apparent that the advantages of velocity overshoot are absent from the 2 μm long calculation. The reason for this is direct: the carriers have traversed a path of sufficient length to exceed the threshold energy for electron transfer. In this case electron transfer results in velocity saturation and currents appropriate to the steady state parameters. Thus, while a blocking contact may be expected to yield high entrance velocities for one species of carriers, electron transfer prevents a large fraction of these carriers from enjoying the speed advantage. The message here is that a forgiving contact is useful only when

coupled to an appropriate device design. Within the framework of the displaced Maxwellian, improvements in device structure are synonymous with values of electron temperature that are below that required for electron transfer.

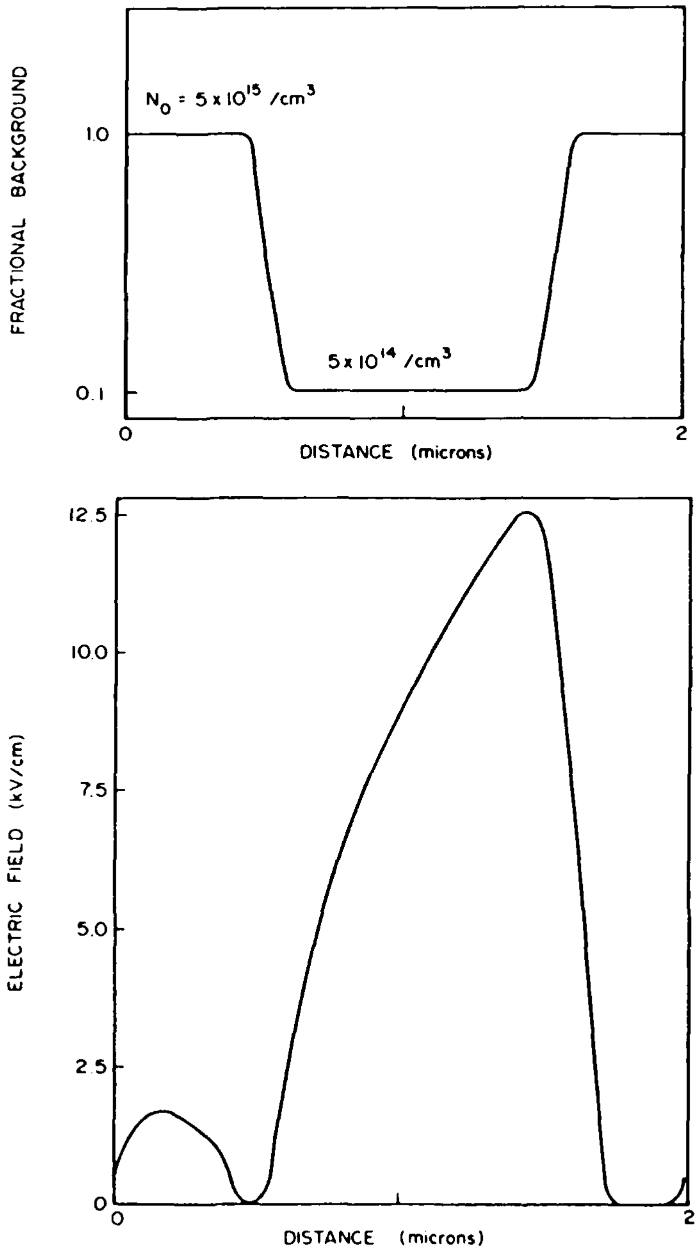

Fig. 14. (a) Doping distribution for N–N$^-$–N device. Bias is 1 V, and conditions at the cathode boundary are as in fig. 9. (b) Electric field distribution.

One way of reducing the electron temperature is simply to go to shorter device structures, and recent results for gallium arsenide at room temperature suggest that device structures not greater than 0.25 μm may be required. A structure that has recently been discussed within the framework of near and submicron devices is the $N-N^{-}-N$ structure shown in fig. 14. This structure has four interfaces to contend with. The most significant aspect of this structure is that it introduces an abrupt change in field at the $N-N^{-}$ interface, which tends to emphasize overshoot contributions. The detailed input to this calculation is as follows. The N region is doped to $5 \times 10^{15}/\mathrm{cm}^3$ with the N^- region an order of magnitude less in doping. For this device the cathode ohmic conditions of fig. 9 were imposed, and an average field of 5 kV/cm was imposed. We note that over a distance of approximately 1.0 μm there is very little electron transfer. Current is carried mainly by Γ-valley electrons whose carrier velocity peaks near 6×10^7 cm/s, showing substantial overshoot. The electron temperature for this calculation is shown in fig. 15, and is reasonably low. V_{av} for this case is 1.3×10^7 cm/s.

The results of this calculation are very encouraging. However, they are not solely a consequence of structural device changes. The retention of Γ-valley electrons in the fig. 15 calculation is a consequence of using an electronic thermal conductivity appropriate to $5 \times 10^{15}/\mathrm{cm}^3$ through the Wiedemann–Franz ratio. A reduction in electronic thermal conductivitiy results in steeper gradients in electron temperature. Fig. 16 shows results for a value of thermal conductivity in which substantial transfer occurs within 0.5 μm of entry into the N^- region. The average current has dropped to 6.5×10^6 cm/s. The first set of results which virtually eliminate transfer must be regarded as an upper bound on current, whereas the second set is a lower bound. Actual device results are likely to fall between the two. One important measurement likely to provide significant information is whether a 1 μm, $10^{14}/\mathrm{cm}^3$ element will show small signal gain.

Returning to the boundary conditions, there are several points to be made. First, there is a clear indication as to the procedures necessary for generating an entire set of "ohmic" and blocking contacts. It is not likely, however, that the boundary prescriptions of figs. 9 to 13 are unique; other sets of conditions can be envisioned to yield similar results under DC conditions. Distinguishing between different boundary condition effects will come from time dependent studies. The question then is: "How model dependent are the results?"

The governing equations are derived starting from the condition of a displaced Maxwellian, which assumes strong electron–electron interaction. Boundary scattering is likely to substantially alter this interaction – near the boundary [25]. Results that appear to be model independent are those associated with the entrance velocity. If central valley carriers enter with speeds greater (less) than that dictated by equilibrium band structure considerations, carrier accumulation (depletion) will occur.

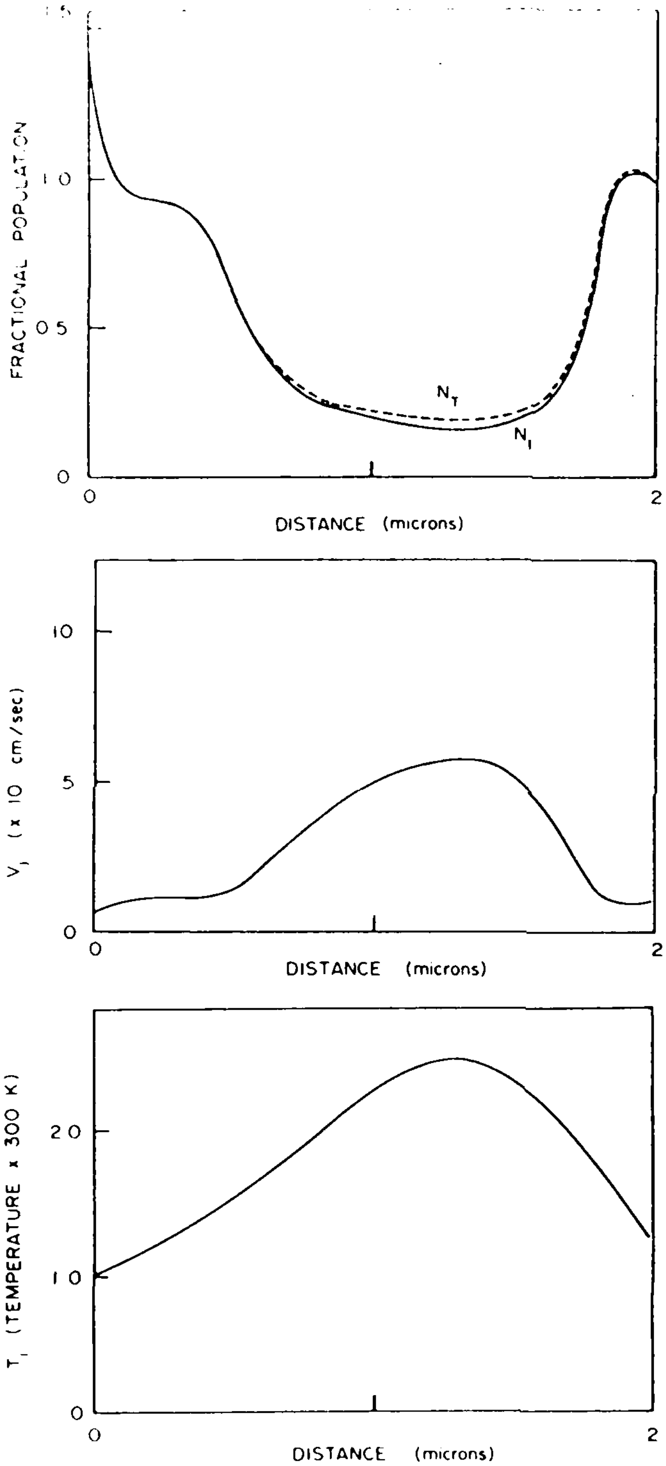

Fig. 15. (a) Fractional population. (b) Central valley velocity. (c) Electron temperature, for calculation of fig. 14.

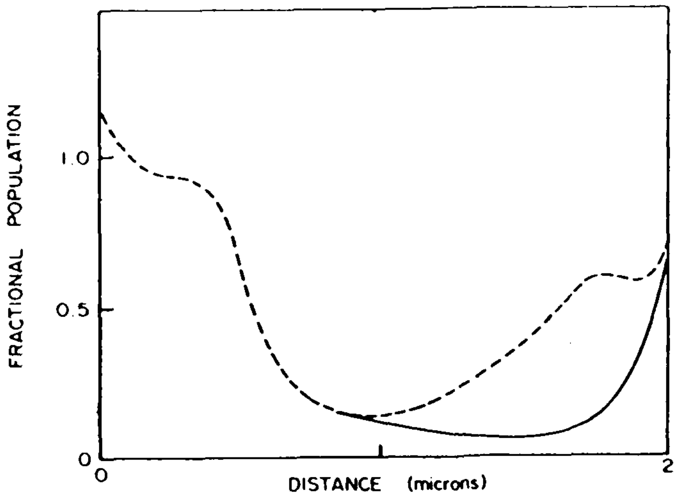

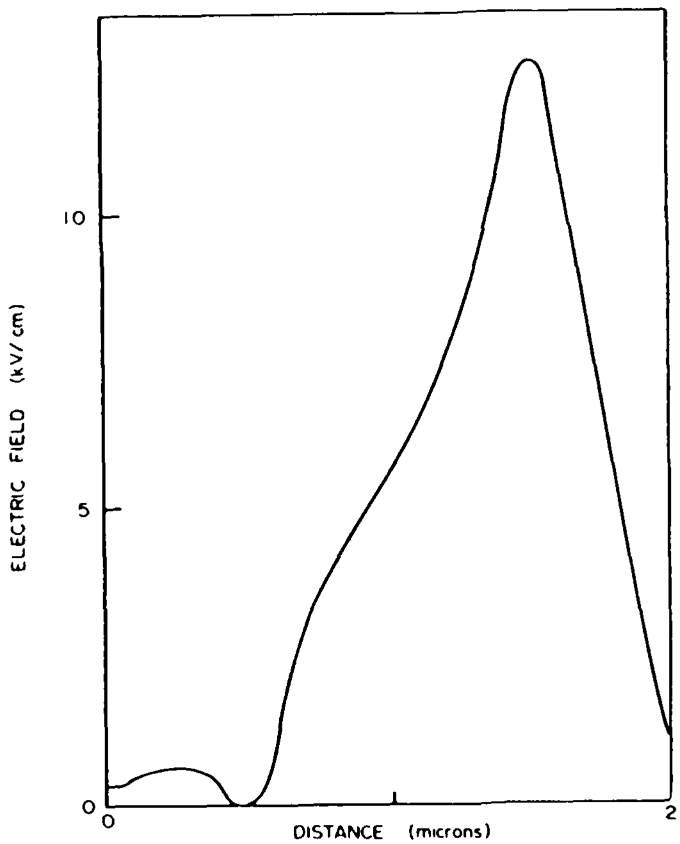

Fig. 16. (a) Fractional population. (b) Electric field distribution, for parameters of fig. 14 with a reduced thermal conductivity.

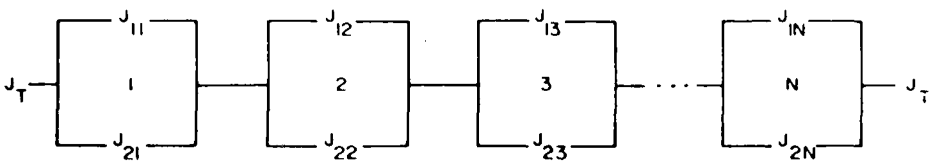

Fig. 17. Representation of spatial dependence of current flow through two level device as a serial chain of parallel elements. The first subscript in each element represents current through the central valley 1 or satellite valley 2.

Another point worth raising, particularly with regard to the absence of overshoot in figs. 9 to 13, is the fact that for at least half of these devices the space distributions were in steady state equilibrium with results similar to those of the drift and diffusion equations. While going to shorter device lengths does not necessarily prevent this from occurring [26], the length dependence has not been explored.

The results of figs. 9 to 13 also suggest that transport in a multivalleyed system may be controlled by one of the valleys. In the above examples, control is by the central valley; satellite valley boundary conditions are relatively benign. To see the reasons for this it is necessary to turn to fig. 17, which represents current flow through the nonlinear elements as a linear chain of parallel resistors. In this figure

$$J_{1i} = N_{1i}V_{1i}, \quad i = 1, 2, \ldots, N,$$

$$J_{2i} = N_{2i}V_{2i}, \quad i = 1, 2, \ldots, N.$$

The voltage across element i is $F_i \Delta X$. Thus if, e.g., the Γ valley in element 1 sustains a net carrier density below the background, it will have a higher resistance and voltage drop than an element with a density closer to background. This, of course, is consistent with the results of fig. 11 and suggests that the portion of the conduction band with boundary conditions most strongly departing from the uniform field conditions will be the dominant boundary condition.

The contact boundary conditions discussed in figs. 9 to 13 address only a small part of the problem. It is certainly unrealistic to assume that undesirable departures in doping will be absent. A simulation of a nominally $10^{17}/\mathrm{cm}^3$ doped device, with a 10% decrease in doping over a distance of 1000 Å, is shown in fig. 18. The distortion in electric field, for the set of boundary conditions listed in the caption, is such as to prevent any real overshoot from occurring.

The above results which reflect the influence of space charge on transport in devices should be compared to uniform field calculations to indicate the goals that perhaps should be taken for some device structures. Fig. 19 displays velocity versus distance curves for electrons subjected to a sudden value of

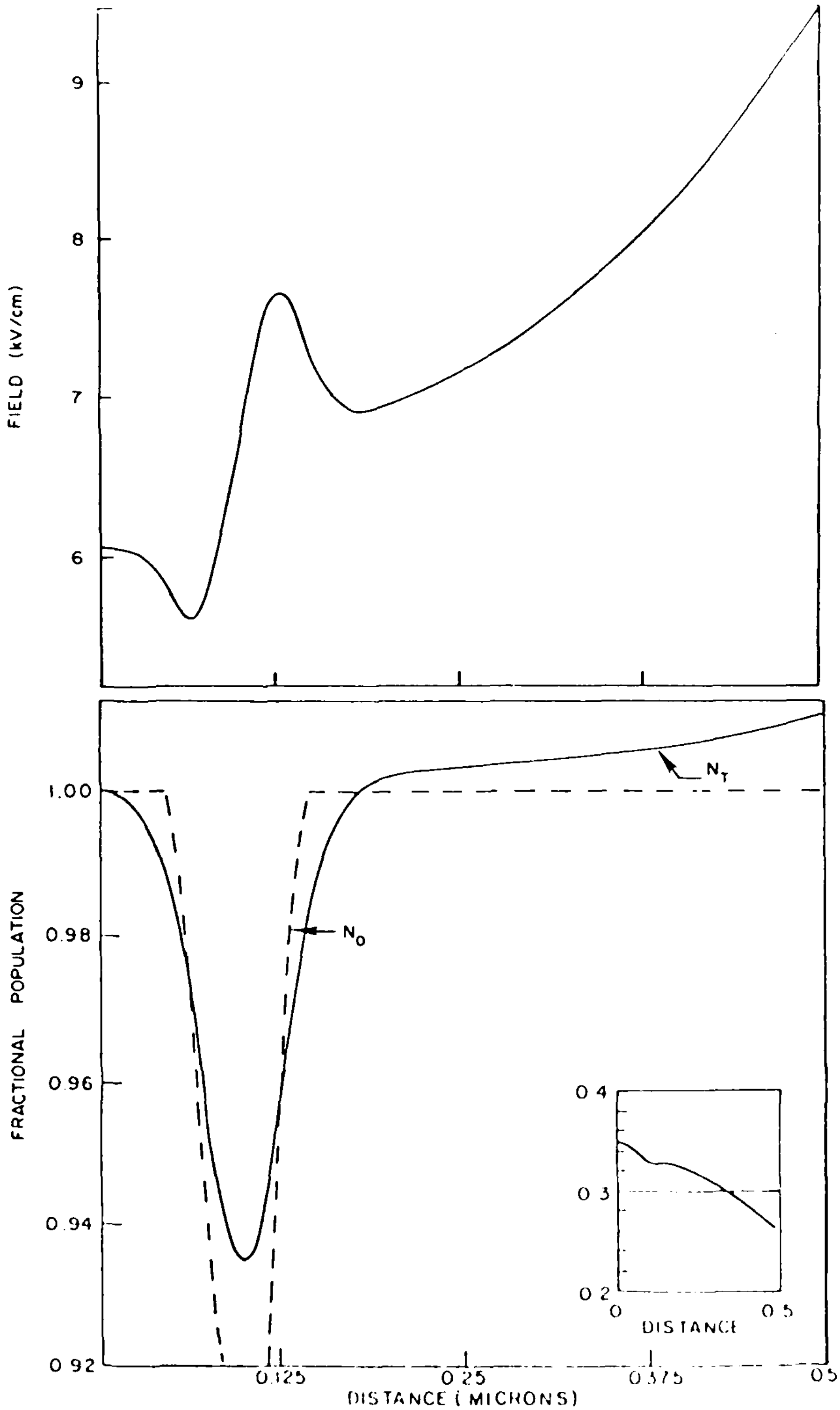

Fig. 18. (a) Electric field versus distance. (b) Carrier density versus distance for a "notched" device. Shown in the inset is the central valley carrier distribution. From ref. [26], with permission.

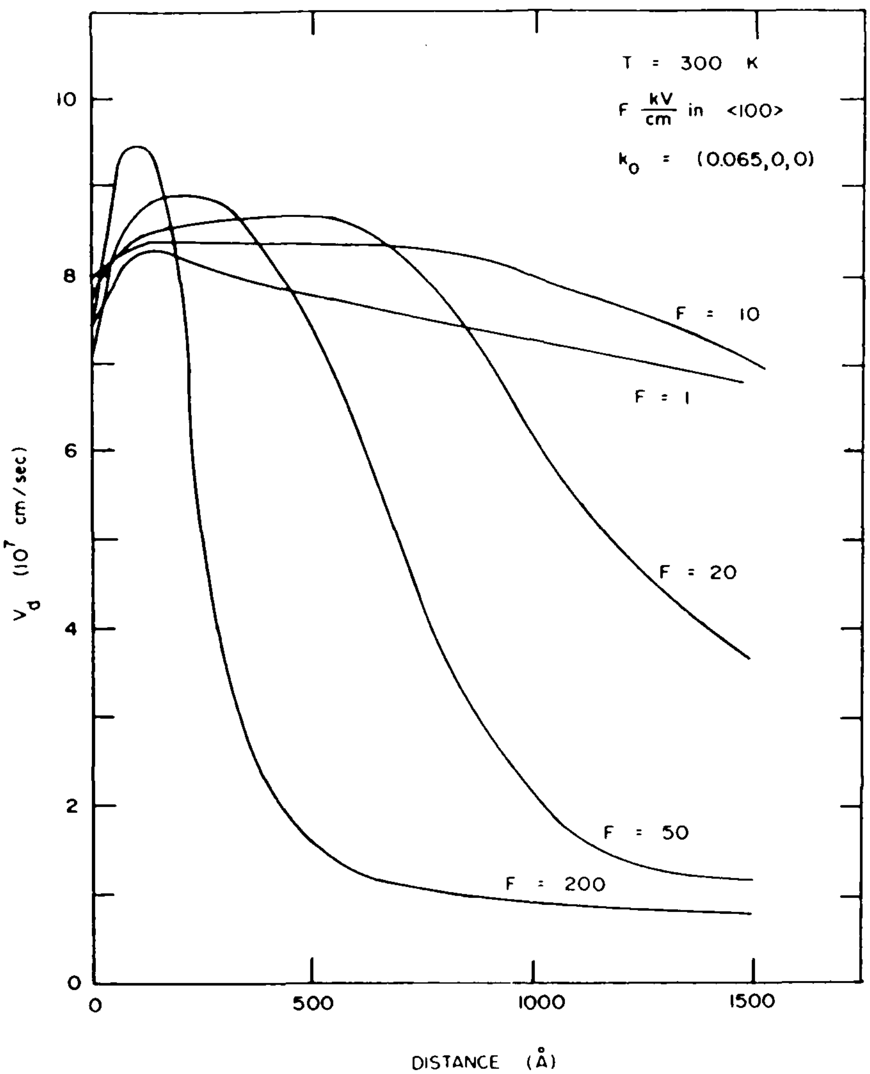

Fig. 19. Velocity versus distance for electrons with a finite entrance energy subjected to a sudden change in electric field. From ref. [27], with permission.

electric field. In this case the energy of the entering carriers is just below that required for electron transfer. It is seen that moderate values of electric field are necessary to sustain high transit velocities. In fig. 20 the dependence of transit velocity on entrance energy is calculated. It is seen that there is a window for high transit velocities, and it is this velocity level that is sought.

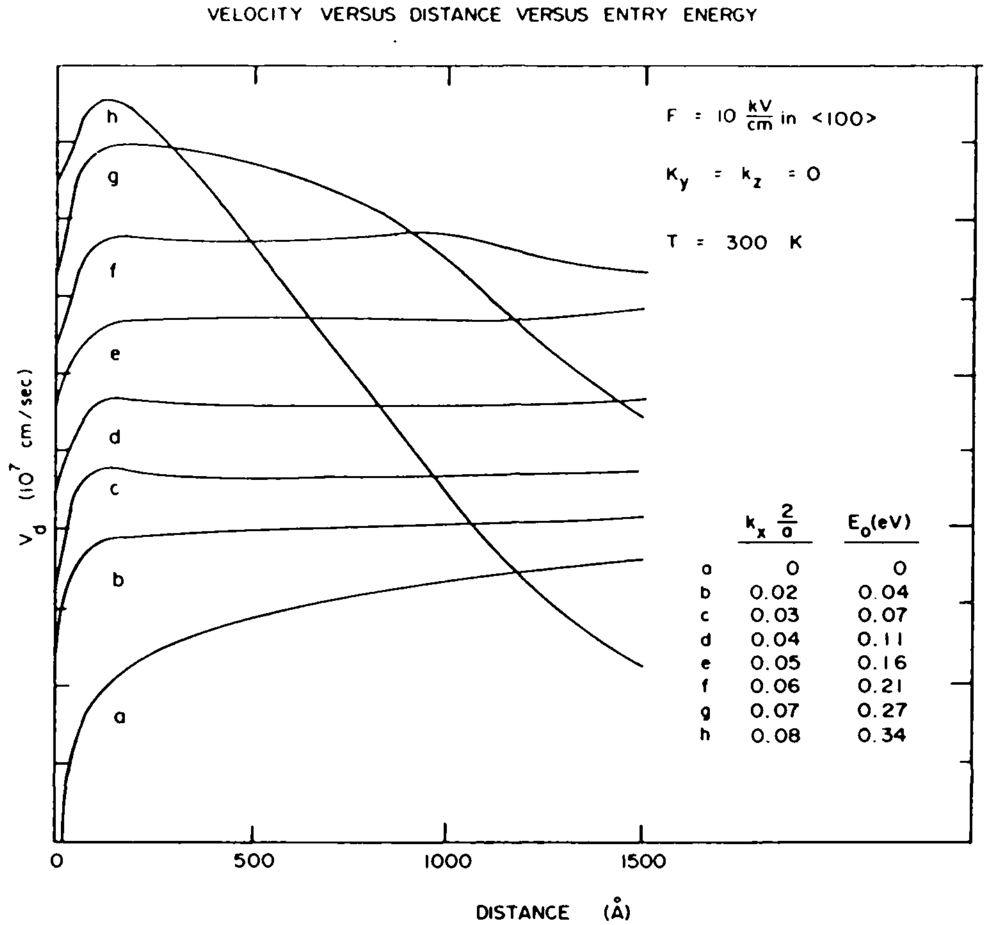

Fig. 20. Velocity versus distance for electrons with varying entrance energies, subject to a sudden change in electric field. From ref. [27], with permission.

4. Summary

The experimental situation is such that, with the exception of long compound semiconductor devices, there are very few data on the role of boundaries and contacts to submicron devices. The reason for the paucity of data lies in the fact that most submicron devices are three terminal device designs and the third terminal tends to mask the role of the contact boundaries. This is extremely unfortunate since it is likely that two terminal device measurements will indicate what can be achieved in controlling the entrance dynamics of the carriers. To date, most two terminal device measurements on simple device structures have concentrated on the role of transport *within* the device, and raise the question of whether "ballistic" motion is possible [28]. Based on the

history of vacuum tube dynamics [29] it should be recalled that, if transport is ballistic, the electrical characteristics will be controlled by the contacts.

The situtation in submicron devices is further complicated by communication between the up- and down-stream contacts. Thus it may be expected that the influence of a blocking contact on the electrical characteristics of long and submicron devices will be different. For submicron devices simple current voltage measurements may be rendered useless as a diagnostic tool. This is certainly not the case in long devices.

The role of numerical simulations in these boundary and device studies has been to act as surrogates for measurements that are not feasible. In one case, obtaining cathode boundary fields from measurements was not possible. Thus for long devices the sensitivitiy of the numerical results to numerical changes in the boundary conditions, when coupled to experiments, provided the key to the role of contacts on device behavior [1]. For submicron devices, the difficulties of direct correlation of experiment with specific transport phenomena are apparent and simulation through parametric studies will provide a key to the role of boundaries. But the description of transport on a submicron scale is still inadequate and the descriptive role of boundaries is correspondingly weak. For example, most space charge dependent problems still treat the background as a "jellium" distribution. The discrete nature of impurities is ignored, as are structural variations in the contacts. The extent to which this affects such measurements as current-versus-voltage is yet to be determined. Notwithstanding these uncertainties, a considerable amount of information can be obtained by extrapolation from the ideal cases which can provide bounds on the limits of transport through both the boundary and active region of the device.

Acknowledgments

The author acknowledges critical discussions with M.P. Shaw, G.J. Iafrate and D.K. Ferry. This work was supported by the Office of Naval Research and the Army Research Office.

References

[1] M.P. Shaw, P.R. Solomon and H.L. Grubin, IBM J. Res. Develop 13 (1969) 587.

[2] D.J. Colliver, K.W. Gray, D.J. Jones, H.D. Rees, G. Gibbons and P.M. White, in: Proc. 4th Intern. Symp. on GaAs and Related Compounds, Boulder, CO, 1972, Inst. Phys. Conf. Ser. 17 (Inst. Phys., London, 1973) p. 286.

[3] W.G. Guion and D.K. Ferry, Appl. Phys. Letters 11 (1967) 337; J. Appl. Phys. 42 (1971) 2502.

[4] K.W. Boer, H.J. Hansch and V. Kummel, Z. Physik 155 (1969) 170;
K.W. Boer and G. Dohler, Phys. Rev. 186 (1969) 793;
see also M.P. Shaw, P.R. Solomon and H.L. Grubin, Solid State Commun. 7 (1969) 1619.

[5] See, e.g., D. Boccon-Gibodi, J.P. André, P. Baudet and J.P. Hallais, IEEE Trans. Electron Devices ED-27 (1980) 1141.
[6] D. Delagebeaudeuf and N.T. Linh, IEEE Trans. Electron Devices ED-28 (1981) 790.
[7] P.R. Solomon, M.P. Shaw, H.L. Grubin and R.D. Kaul, IEEE Trans. Electron Devices ED-22 (1975) 127.
[8] W.S.C. Gurney, Electron. Letters 7 (1971) 711;
see also K.W. Böer and G. Dohler, Phys. Rev. 186 (1969) 793.
[9] E.M.Conwell, IEEE Trans. Electron Devices ED-17 (1970) 262.
[10] M.P. Shaw, P.R. Solomon and H.L. Grubin, The Gunn–Hilsum Effect (Academic Press, New York, 1979).
[11] H.D. Rees, in: Metal–Semiconductor Contacts, Inst. Phys. Conf. Ser. 22 (Inst. Phys., London, 1974).
[12] H. Kroemer, IEEE Trans. Electron Devices ED-15 (1968) 819.
[13] V.L. Rideout, Solid State Electron. 18 (1975) 541.
[14] H.L. Grubin, R.F. Greene and G.J. Iafrate, to be published.
[15] W. Shockley, J.A. Copeland and R.P. James, Quantum Theory of Atoms, Molecules and the Solid State (Academic Press, New York, 1966).
[16] H.W. Thim, Electron. Letters 7 (1971) 106.
[17] T. Kurosawa, J. Phys. Soc. Japan Suppl. 21 (1966) 424.
[18] H.D. Rees, Solid State Commun. 26A (1968) 416; J. Phys. C5 (1972) 64.
[19] R. Bosch and H. Thim, IEEE Trans. Electron Devices ED-21 (1974) 16.
[20] See, e.g., A. Sommerfeld, Thermodynamics and Statistical Mechanics (Academic Press, New York, 1956) section 43.
[21] H.L. Grubin, D.K. Ferry, G.J. Iafrate and J.R. Barker, in: VLSI Electronics, Vol. 3 (Academic Press, New York, 1982) p. 198.
[22] H.L. Grubin and D.K. Ferry, J. Vacuum Sci. Technol. 19 (1981) 540.
[23] H.L. Grubin, D.K. Ferry and J.R. Barker, in: Proc. 1979 IEDM (1979) p. 394.
[24] B. Faugemberg, M. Pernisek and E. Constant, in: Proc. 1982 Workshop on the Physics of Submicron Structures, to be published.
[25] R.F. Greene, H.L. Grubin and G.J. Iafrate, in: Proc. 1982 Workshop on the Physics of Submicron Structures, to be published.
[26] H.L. Grubin, G.J. Iafrate and D.K. Ferry, in: Proc. 1981 IEDM (1981) p. 633.
[27] G.J. Iafrate, R. Malek, K. Hess and J. Tang, to be published.
[28] M.S. Shur and L.F. Eastman, IEEE Trans. Electron Devices ED-26 (1979) 1977.
[29] See, e.g., H.F. Ivey, Advan. Electron. Electron Phys. 6 (1959) 138.

PHYSICS AND MODELING CONSIDERATIONS FOR VLSI DEVICES

H.L. Grubin & J.P. Kreskovsky

Scientific Research Associates, Inc.
Glastonbury, Connecticut 06033

G.J. Iafrate

U.S. Army Electronics Technology & Devices Laboratory
Fort Monmouth, New Jersey 07703

D.K. Ferry

Colorado State University
Fort Collins, Colorado 80521

R.F. Greene

Naval Research Laboratory
Washington, D.C. 20375

ABSTRACT

Recent results concerning spatial and temporal transport in submicron devices identify significant aspects of the role of boundary conditions, scaling for suggesting new materials, and structural device changes. These results are discussed as a means of achieving high speed and high frequency devices.

INTRODUCTION

There are several recent results concerning spatial and temporal transport in submicron devices that are likely to have an impact on the design of future high frequency sources. These results, which emerge from Monte Carlo, and momentum moment equation solutions to the "Wigner-Boltzmann" quantum transport equation[1]

$$\frac{\partial f_w}{\partial t} + \frac{p}{m}\frac{\partial f_w}{\partial x} - \frac{2}{\hbar}\{\sin\frac{\hbar}{2}(\frac{\partial}{\partial x}\frac{\partial}{\partial p})\}V(x)f_w(x,p) = (\frac{\partial f_w}{\partial t})_{coll}, \quad (1)$$

and the Boltzmann transport equation (BTE)

$$\frac{\partial f}{\partial t} + \frac{p}{m}\frac{\partial f}{\partial x} + \dot{p}\frac{\partial f}{\partial p} = (\frac{\partial f}{\partial t})_{coll}, \quad (2)$$

identify crucial aspects of boundary conditions, the role of scaling in choosing suitable materials, and the significance of alterations in otherwise simple device structures for achieving high speeds. These topics are reviewed below. (It is noted: In equation (1) the position gradient in the brackets operates only on the potential energy, f_w is a single coordinate and momentum distribution function

$$f_w(x,p) = \frac{1}{2\pi\hbar}\int dy\Psi^* (x + \frac{y}{2})\ \Psi\ (x - \frac{y}{2})e^{ipy/\hbar} \quad (3)$$

and $\Psi(x)$ represents the state of the system in the coordinate representation).

SCATTERING MODIFICATIONS TO BALLISTIC TRANSPORT

Ballistic transport implies carrier transport unimpeded by inter actions (electrostatic, or otherwise) with other carriers, or with scattering events. The extent to which scattering centers are sensed by transiting electrons is therefore of significance. The first set of calculation shown, Figure 1 (Ref. 2), represents scattering events in GaAs for a collection of electrons entering a uniform field region with an initial energy of approximately 0.30ev. Intervalley Γ-L ener separation for this Monte Carlo calculation is 0.33ev. It is seen that, with the exception of very high fields, approximately 50% of th carriers are unscattered over the first 500°A.

The velocity versus distance curves for this calculation are dis played in Figure 2 (Ref 2), and it is seen that high speeds over useful distances can be achieved even in regions where a high number of scattering events has occured. The optimum conditions for this appear to require moderate fields, generally near the threshold field for electron transfer, and moderate injection energies. The dependence on the latter is displayed in Figure 3 (Ref.2), where the lowest achievable velocities over a distance of 1500°A are for entry electrons with zero initial velocity. It is also seen that an optimum

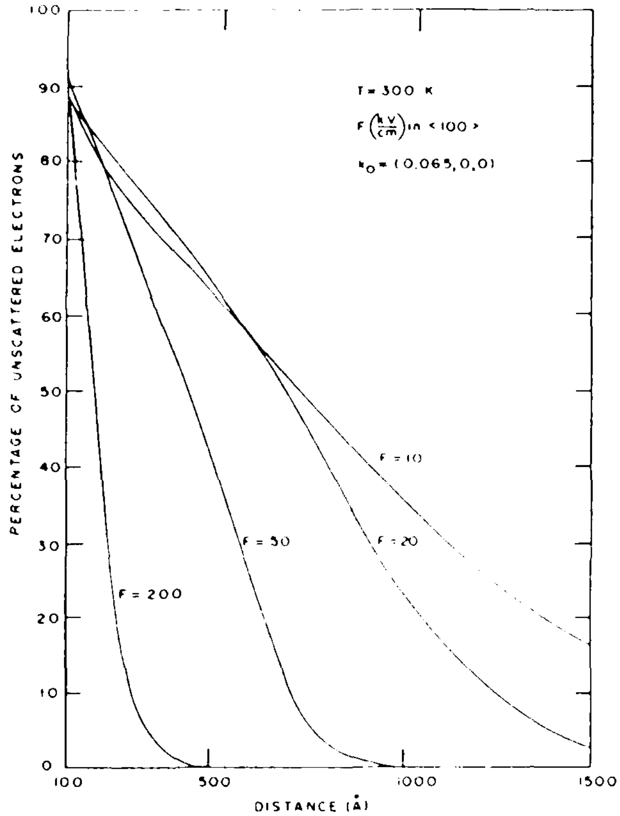

Figure 1. Percentage of unscattered electrons versus distance. Entrance electrons have a finite energy. From reference 2, with permission.

entry energy exists; for energies near the Γ-L separation, scattering quickly reduces the net drift velocity. The optimum conditions identified by these calculations imply that voltage control near the entrance boundary must be near 50mv.

The examples of Figures 1 through 3 are for uniform fields, and carriers subject to sudden changes in field. Studies in which spatial gradients accompany nonuniform fields are more recent, several of which are considered at this Workshop. One aspect is considered below.

SPATIAL AND TEMPORAL TRANSIENTS

A relatively direct way of handling spatial and temporal transients is through moments of the transport equations (1) and (2). Little has been done with the moments to the Wigner - Boltzmann equation and the following deals exclusively with BTE moments. The moments of the BTE form an infinite hierarchy of moment equations. Each equation introduces a higher order moment not defined by the

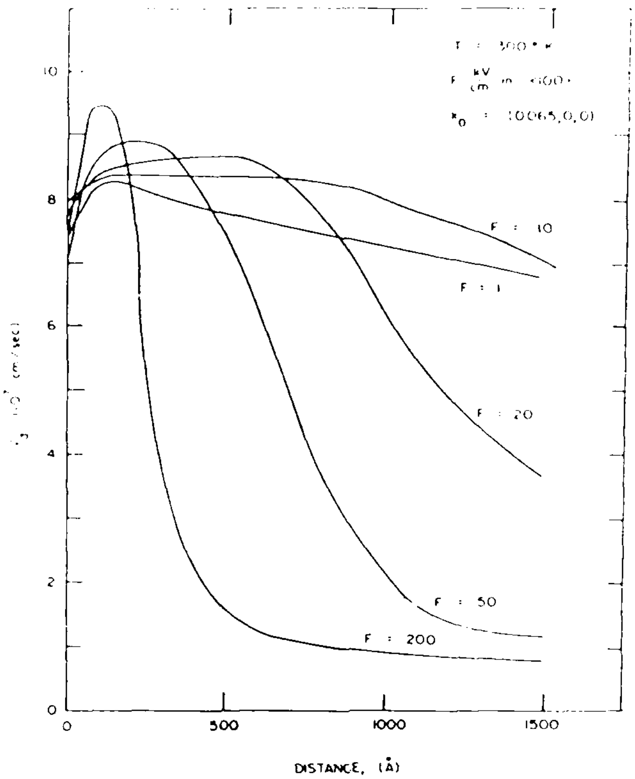

Figure 2. Velocity versus distance for electrons with a finite entrance energy subject to a sudden change in electric field. From reference 2, with permission.

given set of balance equations. The most common form of the balance equations is obtained by assuming a distribution function of the form

$$f = f_{oi} \sim \frac{n_i}{T_i^{3/2}} \exp - \left\{ \frac{m(u-v)^2}{2\, k_o T_i} \right\} \tag{4}$$

for each species. More generally (Ref. 4)

$$f = \left(1 + A_k \frac{\partial}{\partial u_k} + A_{kl} \frac{\partial^2}{\partial u_k \partial u_l} + A_{klm} \frac{\partial^3}{\partial u_k \partial u_l \partial u_m} + \ldots \right) f_o \tag{5}$$

where it is insisted that the first term in the expansion gives the correct local values of density, velocity and energy. The coefficients in the above expansion are inversely proportional to density and are model dependent. The first correction to the local equilibrium balance equations, the so-called hydrodynamic approximation yielc

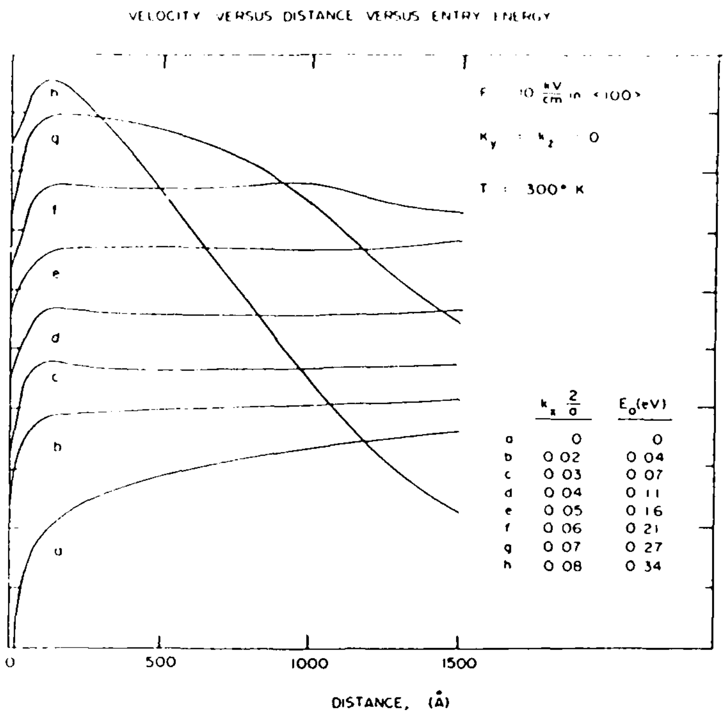

Figure 3. Velocity versus distance for electrons with varying entrance energies subject to a sudden change in electric field. From reference 2, with permission.

$$\frac{\partial n_i}{\partial t} + \nabla \cdot (\vec{v}_i n) = \left(\frac{\partial n_i}{\partial t}\right)_{coll} \tag{6}$$

$$\frac{\partial \vec{P}_i}{\partial t} + \nabla \cdot (\vec{v}_i \vec{P}_i) = -en_i \vec{F} - \text{grad } n_i k_o T_i - \boxed{\text{div } \overleftrightarrow{\sigma}} + \left(\frac{\partial P_i}{\partial t}\right)_{coll} \tag{7}$$

$$\frac{\partial}{\partial t} W_i + \nabla \cdot \vec{v}_i W_i = -en_i \vec{F} \cdot \vec{v}_i - \nabla \cdot v_i n_i k_o T_i - \boxed{\text{div } \overleftrightarrow{\sigma}^i \times v_i} \tag{8}$$

$$+ \boxed{\text{div } (\kappa \text{ grad } T)} + \left(\frac{\partial W_i}{\partial t}\right)_{coll}$$

where $P_i = n_i m_i \vec{v}_i$, $W_i = n_i \{\frac{1}{2} m_i v_i^2 + \frac{3}{2} n_i k T_i\}$, $\overleftrightarrow{\sigma}$ is a stress tensor arising from nonuniform velocity distributions, and κ is the thermal conductivity. The stress term is dissipative in that when a nonuniform velocity distribution is impressed on an electron stream there will be reactive forces tending to smooth them out. Detailed information regarding suitable values for these terms are not available, and they are regarded as phenomenological entries; they and their modification by the collision terms are to be studied.

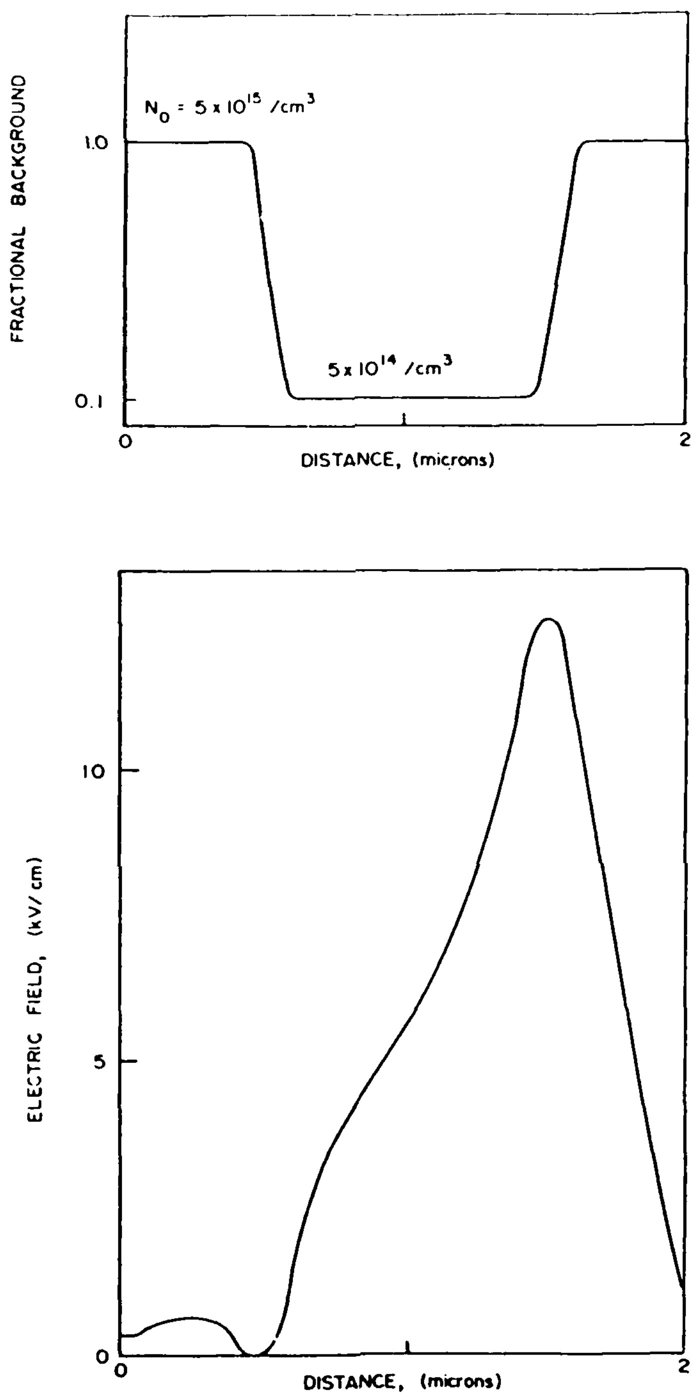

Figure 4. a. Doping distribution for an N^+-N^--N^+ advice. b. Sel
consistent electric field for a bias of 1 volt. (From R
4, with permission).

The boxed terms above represent contributions arising from the nonspherical nature of the distribution function. The underlined terms are ignored in the drift and diffusion approximation. Figure 4 shows the result of a solution to the balance equations for two level transfer for a two-terminal device whose structure is receiving considerable attention as an illustration of velocity overshoot. The structure considered here consists of a low doped region $L \sim 1\mu m$ sandwiched between two regions of higher doping concentration. The structure is subject to a bias of 1 volt. Four interfaces are involved but most attention is focused on the two interior faces where significant gradients in field occur, all associated with differences between the background and mobile carrier density. The carrier concentration is displayed in figure 4c, for the case of injecting cathode contacts (Ref. 4). It is seen that (a) significant charge injection is present in the low doped region, and (b) electron transfer occurs near the downstream section of the low doped region and is significant in the downstream N^+ region. It is noted that the field dependence of carrier density in the Γ valley, $N_\Gamma(F)$ is not the same as that associated with uniform field steady state values. Spatial gradients result in a spatial lag.

Also shown in figure 4c is the drift velocity of carriers in the Γ-valley, and it is apparent that the carriers acquire speeds considerably in excess of the steady state peak velocity of electrons in GaAs. These velocities are not, however, much different in value than those associated with Γ valley electrons under uniform field conditions. The velocity shown in figure 4c is not, however the same as the carrier velocity computed under uniform field conditions. The velocities computed here include temperature as well as momentum gradients, and are properly defined as the current flux/carrier density. Thus, increased velocity here is often associated with decreased carrier density, through current continuity. The key to all device design is that high velocities must be accompanied by only marginal transfer out of the high mobility section of the conduction band. This will require device lengths shorter than the active region of the device shown in this figure. (Modifications to this statement arising from variations in material parameters are considered in Ref. 4).

The calculations of figure 4 show the situation where a high carrier velocity occurs near the downstream edge of the low doped region. Often high velocities are required near the upstream boundary as indicated by figures 1 through 3. Figure 5 (Ref. 6) shows a spatially dependent result for carriers subjected to a prespecified value of electric field. The calculation is for silicon and the highest carrier velocities occur near the 0.4μm boundary. An accompanying plot of carrier density (Ref. 6, figure 9) shows the lowest level of carrier density in the region of highest velocity.

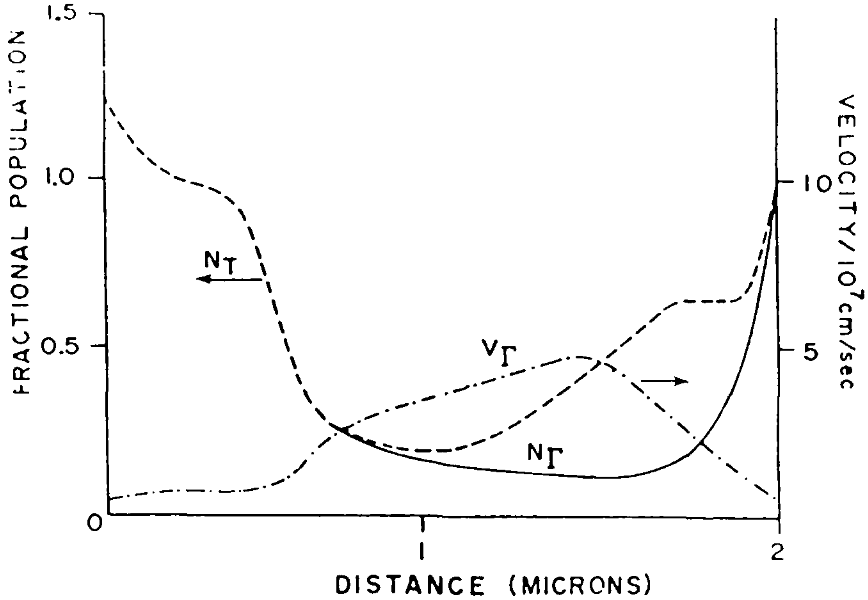

Figure 4C. Fractional population and central value velocity. (Fr Ref. 4., with permission.)

Coupling the above results to the need for moderate fields for high speed operation a useful multiterminal device very likely will require the presence of a local moderate field region that "kicks" electrons into high speed regions. The simplest high field injecting region could come from local charge depletion or "notches" (Fig. 6). Note that in Figure 6 the gate is treated generically. It could be a metal Schottky contact, a p^+ AlGaAs layer, etc.

SCALING

In the absence of, or in concert with structural variations in devices it is also necessary to examine changes in material paramet The change in material parameters should have as its goal high mobil ity and high characteristic velocities. Thornber (Ref. 8) provided general set of guidelines for choosing material parameters through an alteration of the scattering rates, one of which is duscussed bel

The collision term in the Boltzmann transport equation is

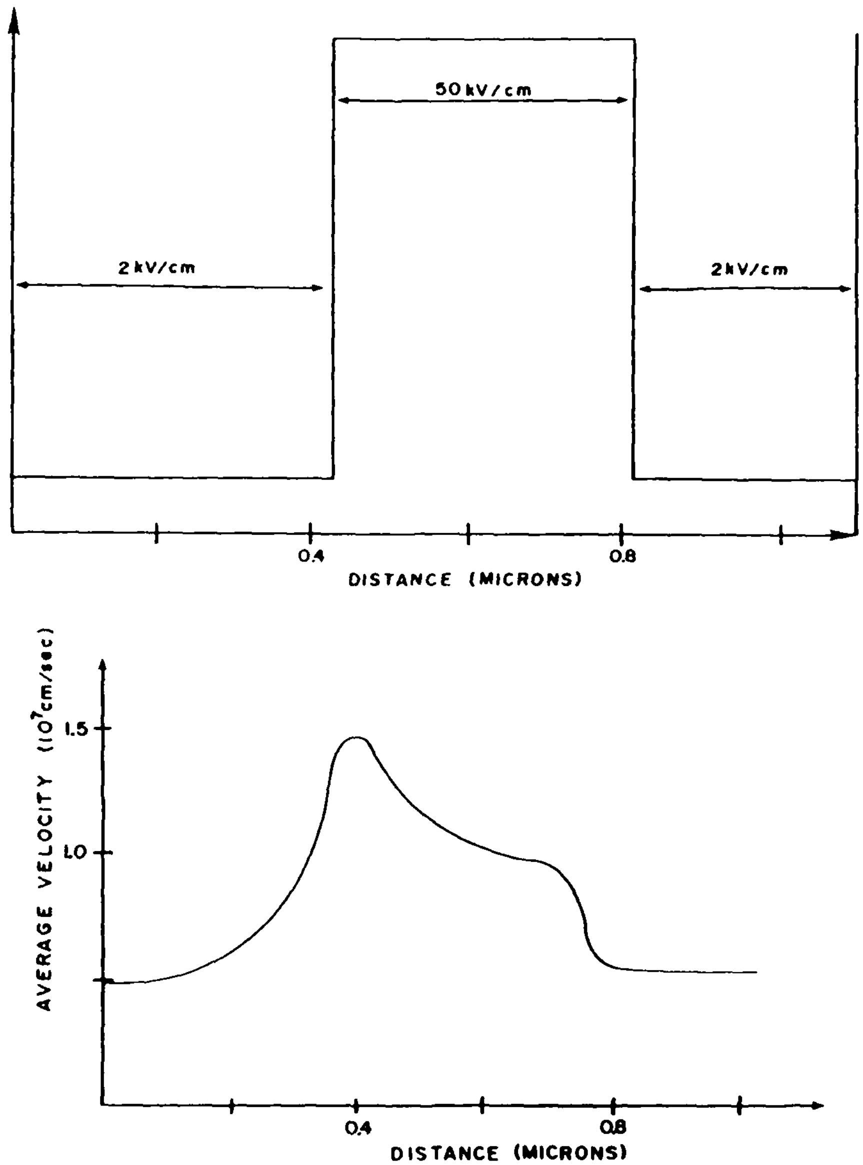

Figure 5. Variation of carrier velocity in silicon for electrons subject to the illustrated field profile. From Ref. 6 with permission

$$\left(\frac{\partial f}{\partial t}\right)_{coll} = \int d^3p' \,\{ f(p')W(p',p) - f(p)W(p,p')\} \tag{9}$$

where $W(p',p)$ is the total scattering rate from $\vec{p}$ to $\vec{p}'$. Thornber suggested several scaling changes in the BTE, to alter the drift velocity.

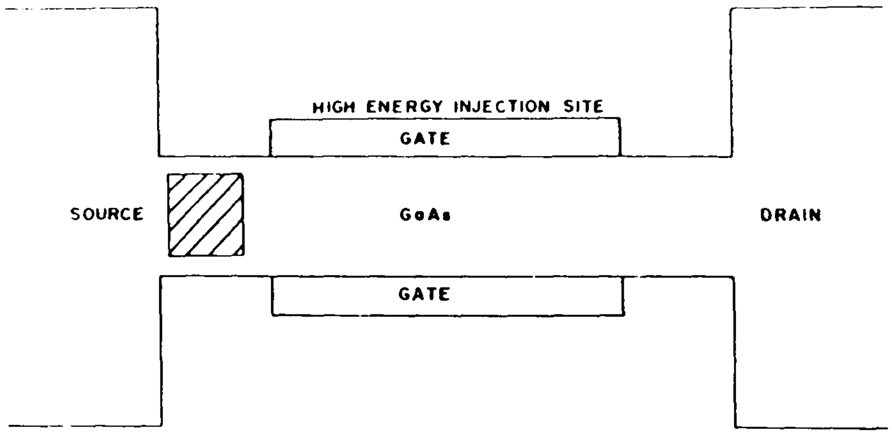

Figure 6. Schematic of a high energy injection region in a gated submicron structure.

$$v = \int d^3 p f \vec{p}/m \int d^3 p f. \quad (10)$$

The one illustrated below involves uniformly altering the scattering rate by a constant Γ, and results in the following relation

$$v_\Gamma(x,t,F) = v(\Gamma x, \Gamma t, F/\Gamma) \quad (11)$$

Where the right-hand side is the unscaled velocity. In this scaling mobility is altered but saturated drift velocity is not.

A dramatic consequence of the effects of scaling is illustrated below, but it is necessary to note that the possibility of relevant material scaling over a broad range of electric field values is remote. Rather, it is more likely to be appliable over a restricted range of field values. This is illustrated for GaAs. For GaAs, over a field range of approximately 3 → 15 kv/cm, intervalley Γ-L coupling is a dominant scattering mechanism. Figure 7 shows the velocity field characteristic for Γ-L-X ordering with three different values of the Γ-L deformation potential. All these valleys are taken as parabolic with N_o=0, while all other material parameters are those of Littlejohn, et al. (Ref.9). (We note that similar values for material constants yield differences between Monte Carlo and balance equation calculations.) In Figure 7 the fields at points 1, 2 and 3 occur at valu 5.6 kv/cm, 8.2 kv/cm and 12 kv/cm, respectively. The dominant Γ valley total momentum scattering rates are 4.78×10^{12}/sec., 7.32×10^{12} sec., and 10.0×10^{12}/sec., respectively. The ratios F/Γ are 1.17×10^{-12}kv-s/cm, 1.12×10^{-12}kv-s/cm and 1.20×10^{-12}kv-s/cm, respectively in general agreement with the rule of Equation 11.

Figure 8 illustrates the consequences of uniform scaling on velocity overshoot. The solid curve displays overshoot for a gallium arsenide element subject to a field of 27kv/cm (Ref. 10). The dashed

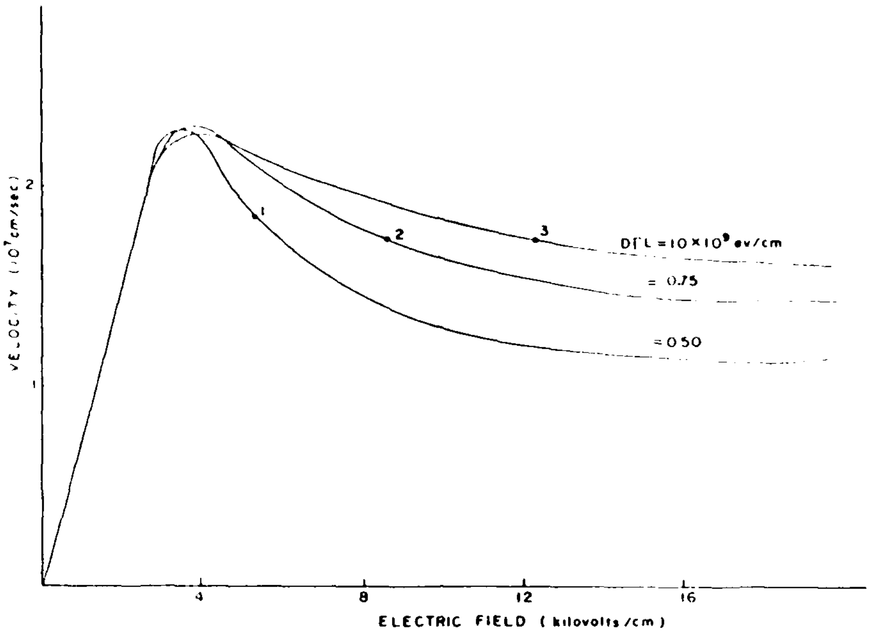

Figure 7. Steady state velocity versus field for Γ-L-X ordering as obtained from balance equations. Different curves are for different values of the deformation potential coupling constant for intervalley Γ-L scattering.

(dotted) curve is a sketch of a scaled curve for Γ≈2(Γ≈0.5) and a field of 54kv/cm (13.5kv/cm). For Γ≈2, high overshoot velocities occur over a short period of time and require high bias levels. By reducing Γ to values below 1.0 high overshoot velocities are retained for a longer period of time and at lower values of field than for GaAs. This result is highly significant insofar as it suggests higher transit velocities for extended temporal scales, and indicates a direction of material selection for high frequency sources.

GENERAL CONCLUSION

It has been known since 1969 that the compound semiconductors, GaAs in particular, are theoretically capable of providing high frequency, near 100GHZ oscillations. Overshoot has also been known since that time (Ref. 11). The difficulty in attaining high frequency three-terminal and sometimes two-terminal operation has over the past decade been attributed to inadequate contact regions (Ref. 12), material preparation, etc. Many of the high frequency problems were thought to be reduced by going to small dimensions, where in addition to shorter transit lengths the benefits of overshoot would emerge. While it is still too early to state how these benefits can be implemented in practice, it is clear that special contacts or injection regions

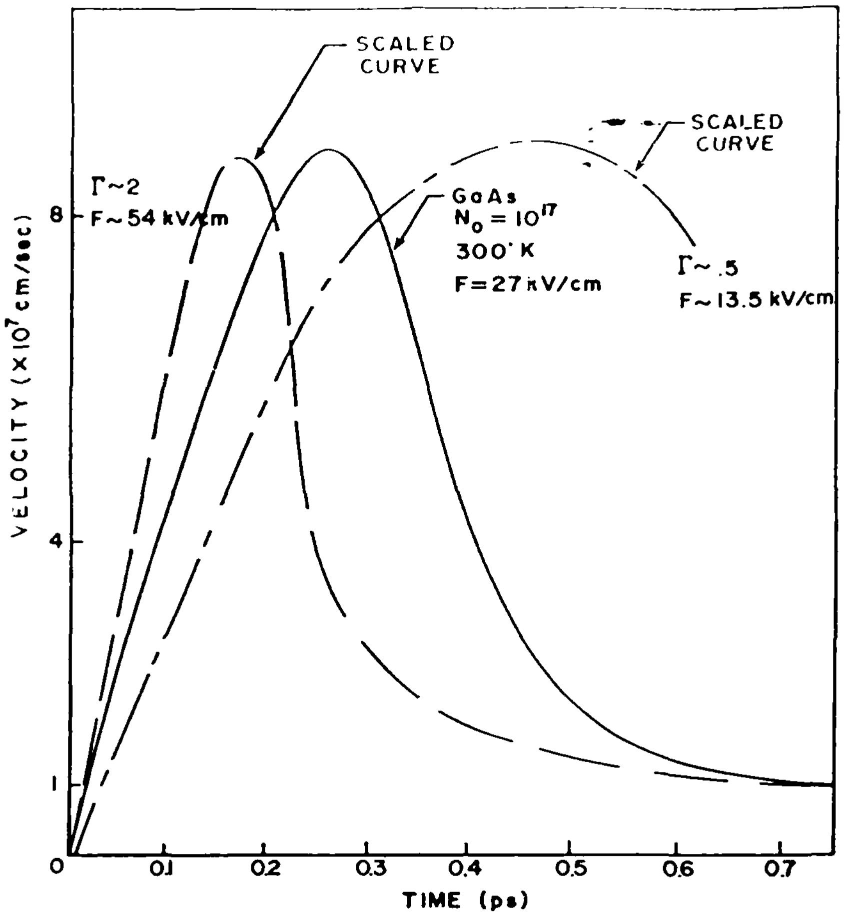

Figure 8. Transient velocity characteristics for scaled and unscaled scattering rates. Solid curve is from reference 10.

are required. It appears, therefore, that the 1969 questions as to why devices are not operating closer to theoretical limits is still valid today. The dual solution approaches of the last decade also appear equally valid today, where the pursuit of novel device structures emphasizing the boundary role is continuing, while simultaneous new material directions are sought.

ACKNOWLEDGEMENT

This work was supported by the Office of Navel Research, and the Army Research Office, to whom we are grateful.

REFERENCES

1. G.J. Iafrate, H.L. Grubin and D.K. Ferry, J. de Physique C7, 307 (1981).
2. G.J. Iafrate, R. Malik, K. Hess and J. Tang. To be published.
3. See, e.g., A. Sommerfeld, Thermodynamics and Statistical Mechanics, Sec. 43. Adacemic Press, NY (1956).
4. H.L. Grubin and J.P. Kreskovsky, Surface Science 39 (1983).
5. H.L. Grubin, G.J. Iafrate and D.K. Ferry, J. de Physique C7, 201 (1981).
6. E. Constant and B. Boittiaux, J. de Physique C7,73 (1981).
7. R.K. Cook and J. Frey, IEEE Trans. Electron Devices, Ed-29 (1982).
8. K. Thornber, J. Appl. Phys. 51, 2127 (1980).
9. M.A. Littlejohn, J.R. Hauser and T.H. Glisson, J. Appl. Phys. 48, 4587 (1978).
10. H.L. Grubin and D.K. Ferry, J. Vac. Sci. & Tech. 19, 540 (1981).
11. P.N. Butcher and C.J. Hearn, Electron. Lett. 4, 459 (1968).
12. M.P. Shaw, H.L. Grubin and P.R. Solomon. The Gunn-Hilsum Effect, Academic Press, NY 1979.

THE WIGNER DISTRIBUTION FUNCTION

G.J. IAFRATE
US Army Electronics Technology and Devices Laboratory (ERADCOM), Fort Monmouth, NJ 07703, USA

H.L. GRUBIN [1]
Scientific Research Associates, Glastonbury, CT 06033, USA

and

D.K. FERRY
Colorado State University, Ft. Collins, CO 80523, USA

Received 17 August 1981
Revised manuscript received 9 October 1981

In this letter, the relationship between the characteristic function for two arbitrary noncommuting observables and a generalized Wigner distribution function is established. This distribution function is shown to have no simple interpretation in the sense of probability theory but, in lieu of its special properties, can be used directly for calculating the expectation values of observables.

Whereas classical transport physics is based on the concept of a probability distribution function which is defined over the phase space of the system, in the quantum formulation of transport physics, the concept of a phase space distribution function is not possible inasmuch as the noncommutation of the position and momentum operators (the Heisenberg uncertainty principle) precludes the precise specification of a point in phase space. However, within the matrix formulation of quantum mechanics, it is possible to construct a "probability" density matrix which is often interpreted as the analog of the classical distribution function.

There is yet another approach to the formulation of quantum transport, based on the construction of the Wigner distribution function [1]. As we shall show, this distribution function has no simple interpretation in the sense of probability theory [2] but, in lieu of its special properties, can be used directly for calculating expectation values [3–5] of observables in a manner quite analogous to that of classical theory, i.e. by integrating the product of the observable and the Wigner distribution function over all phase space.

This letter, in part, reviews the salient features of the Wigner distribution function. Although the Wigner function is generally defined in terms of all the generalized coordinates and momenta of the system in question as

$$P_{\mathrm{W}}(x_1 \dots x_n, p_1 \dots p_n) = \frac{1}{2\pi\hbar} \int_{-\infty}^{\infty} \mathrm{d}y_1 \dots \mathrm{d}y_n \times \Psi^*(x_1 + \tfrac{1}{2}y_1, \dots x_n + \tfrac{1}{2}y_n) \times \Psi(x_1 - \tfrac{1}{2}y_1, \dots x_n - \tfrac{1}{2}y_n) \times \exp[\mathrm{i}(p_1 y_1 + \dots + p_n y_n)/\hbar] , \quad (1)$$

we will discuss the properties of the Wigner function in terms of a single coordinate and momentum. In this case, we let

[1] Partially supported by the Army Research Office.

$$P_W(x,p)=\frac{1}{2\pi\hbar}\int_{-\infty}^{\infty} dy\, \Psi^*(x+\tfrac{1}{2}y)\Psi(x-\tfrac{1}{2}y)e^{ipy/\hbar}, \quad (2)$$

where $\Psi(x)$ refers to the state of the system in the coordinate representation.

The distribution function of eq. (2) has interesting properties in that the integration of this function over all momenta leads to the probability density in real space; conversely, the integration of this function over all coordinates leads to the probability density in momentum space. In mathematical terms,

$$\int_{-\infty}^{\infty} P_W(x,p)\, dp = \Psi^*(x)\Psi(x) \quad (3a)$$

and

$$\int_{-\infty}^{\infty} P_W(x,p)\, dx = \phi^*(p)\phi(p)\,, \quad (3b)$$

where

$$\phi(p)=(2\pi\hbar)^{-1/2}\int_{-\infty}^{\infty} e^{-ipx/\hbar}\Psi(x)\, dx\,.$$

It follows immediately from eq. (3) that, for an observable $W(x,p)$ which is either a function of momentum operator alone or of position operator alone, or any additive combination therein, the expectation value of the observable is given by

$$\langle W\rangle = \iint W P_W(x,p)\, dx\, dp\,, \quad (4)$$

which is analogous to the classical expression for the average value. Herein lies the interesting aspect of the Wigner distribution function; the result of eq. (4) suggests that it is possible to transfer many of the results of classical transport theory into quantum transport theory by simply replacing the classical distribution function by the Wigner distribution function. However, unlike the density matrix, the Wigner distribution function itself cannot be viewed as the quantum analog of the classical distribution function since it is generally not positive definite and nonunique [$P_W(x,p)$ of eq. (2) is not the only bilinear expression [1,3–5] in Ψ that satisfies eq. (3)].

Further resemblance of the Wigner distribution function to the classical distribution function is apparent by examining the equation of time evolution for $P_W(x,p)$. Upon assuming that $\Psi(x)$ in eq. (2) satisfies the Schrödinger equation for a system with hamiltonian $H=p^2/2m+V(x)$, it can be readily shown that $P_W(x,p)$ satisfies the equation

$$\partial P_W/\partial t + (p/m)\,\partial P_W/\partial x + \theta\cdot P_W = 0\,, \quad (5)$$

where

$$\theta\cdot P_W = -\frac{2}{\hbar}\sum_{n=0}^{\infty}(-1)^n\frac{(\hbar/2)^{2n+1}}{(2n+1)!} \times \frac{\partial^{2n+1}V(x)}{\partial x^{2n+1}}\,\frac{\partial^{2n+1}P_W(x,p)}{\partial p^{2n+1}}. \quad (6)$$

It is evident that in the limit $\hbar\to 0$, $\theta\cdot P_W$ in eq. (6) becomes

$$\theta\cdot P_W = -(\partial V/\partial x)(\partial P_W/\partial p) \quad (7)$$

so that eq. (5) reduces to the classical collisionless Boltzmann equation.

The Wigner distribution function defined in eq. (2) is derivable [6] from the Fourier inversion of the expectation value (with respect to state $\Psi(x)$ of the operator $e^{i(\tau\hat{p}+\theta\hat{x})}$ (here, $\hat{x}$ and $\hat{p}$ satisfy the commutation relation $[\hat{x},\hat{p}]=i\hbar$). As such,

$$P_W(x,p)=\frac{1}{4\pi^2}\iint C_W(\tau,\theta)e^{-i(\tau p+\theta x)}d\tau\, d\theta\,, \quad (8a)$$

where

$$C_W(\tau,\theta)=\int \Psi^*(x)e^{i(\tau\hat{p}+\theta\hat{x})}\Psi(x)\, dx\,, \quad (8b)$$

and the interval of integration is $(-\infty,\infty)$ unless otherwise specified. In order to show that the right-hand side of eq. (8a) is indeed the Wigner distribution function as defined in eq. (2), note, from the Baker–Hausdorff theorem [7], that $e^{i(\tau\hat{p}+\theta\hat{x})}$ can be written as

$$e^{i(\tau\hat{p}+\theta\hat{x})}=e^{i\tau\hat{p}/2}e^{i\theta\hat{x}}e^{i\tau\hat{p}/2}\,, \quad (9)$$

in which case $C_W(\tau,\theta)$ of eq. (8b) becomes

$$C_W(\tau,\theta)=\int_{-\infty}^{\infty}[e^{-i\tau\hat{p}/2}\Psi(x)]^*e^{i\theta\hat{x}}[e^{-i\tau\hat{p}/2}\Psi(x)]\, dx\,, \quad (10)$$

which further reduces to

$$C_W(\tau,\theta)=\int_{-\infty}^{\infty}\Psi^*(x-\tfrac{1}{2}\tau h)e^{i\theta x}\Psi(x+\tfrac{1}{2}\tau h)\,dx\,. \quad (11)$$

Then, by inserting $C_W(\tau,\theta)$ of eq. (11) into the right-hand side of eq. (8a), integrating over the variable θ by using the relation

$$\int_{-\infty}^{\infty} e^{i\theta(x'-x'')}\,d\theta = 2\pi\delta(x'-x'')\,,$$

and letting $\tau=-y/h$, the desired result is obtained.

The method outlined above to arrive at the Wigner distribution function is based on the notion of a characteristic function. The characteristic function of an observable, A, with respect to state $|\Psi\rangle$ (here, the Dirac notation is utilized for purposes of generality) is defined as

$$C_A(\xi)=\langle\Psi|e^{i\xi\hat{A}}|\Psi\rangle\,, \quad (12)$$

where ξ is a real parameter. Assuming $\hat{A}$ to possess an eigenvalue spectrum given by $\hat{A}|A'\rangle=A'|A'\rangle$, $C_A(\xi)$ can be evaluated in the A'-representation as

$$C_A(\xi)=\int dA'\int dA''\langle\Psi|A'\rangle\langle A'|e^{i\xi\hat{A}}|A''\rangle\langle A''|\Psi\rangle\,. \quad (13)$$

Since $\langle A'|e^{i\xi\hat{A}}|A''\rangle = e^{i\xi A'}\delta(A'-A'')$ in the A'-representation, $C_A(\xi)$ in eq. (13) reduces to

$$C_A(\xi)=\int dA' e^{i\xi A'}|\Psi_{A'}|^2\,, \quad (14)$$

where $|\Psi_{A'}|^2=|\langle A'|\Psi\rangle|^2 \equiv P(A')$, the probability distribution function for measuring A' while in state $|\Psi\rangle$. Hence, the characteristic function for $\hat{A}$ is the Fourier transform of the probability distribution function $P(A')$. Subsequent inversion of eq. (14) above leads to

$$P(A')=\frac{1}{2\pi}\int C_A(\xi)e^{-i\xi A'}\,d\xi\,. \quad (15)$$

The Wigner distribution function was derived by taking the Fourier transform of the characteristic function for $e^{i(\tau\hat{p}+\theta\hat{x})}$. In view of the connection between the probability distribution function and the characteristic function for a given observable, this approach seems to be a natural way of obtaining a distribution function for momentum and position. Unfortunately, the noncommutative nature of the two observables destroys the convenient probability interpretation of the characteristic function implicit in eq. (15).

In order to demonstrate this point, assume the characteristic function for two noncommuting observables, $\hat{A}$ and $\hat{B}$, to be

$$C_{AB}(\xi_1\xi_2)=\langle\Psi|e^{i(\xi_1\hat{A}+\xi_2\hat{B})}|\Psi\rangle\,. \quad (16)$$

Observables $\hat{A}$ and $\hat{B}$ are assumed to have eigenvalue spectra

$$\hat{A}|A'\rangle=A'|A'\rangle\,,\quad \hat{B}|B'\rangle=B'|B'\rangle\,, \quad (17)$$

and are chosen so that $[\hat{A},[\hat{A},\hat{B}]]=[\hat{B},[\hat{A},\hat{B}]]=0$. This assumption is imposed so that the identity

$$e^{i(\xi_1\hat{A}+\xi_2\hat{B})}=e^{i\xi_1\hat{A}}\,e^{i\xi_2\hat{B}}\,e^{-\xi_1\xi_2[\hat{A},\hat{B}]/2} \quad (18)$$

may be used.

Inserting eq. (18) into eq. (16) while obtaining the matrix elements of $e^{i\xi_1\hat{A}}$ in the A'-representation and $e^{i\xi_2\hat{B}}$ in the B'-representation results in

$$C_{AB}(\xi_1\xi_2)=e^{-\xi_1\xi_2[\hat{A},\hat{B}]/2}\int dA'\int dB' \times e^{i(\xi_1A'+\xi_2B')}\langle\Psi|A'\rangle\langle A'|B'\rangle\langle B'|\Psi\rangle\,. \quad (19)$$

In eq. (19), it is assumed that $[\hat{A},\hat{B}]$ is a c-number independent of the eigenvalues A' and B'. We define $F(A',B')$, the generalized Wigner distribution function [‡1], to be

$$F(A',B')=\langle\Psi|A'\rangle\langle A'|B'\rangle\langle B'|\Psi\rangle\,, \quad (20)$$

so that

$$F(A',B')=\frac{1}{(2\pi)^2}\int d\xi_1\int d\xi_2\, e^{\xi_1\xi_2[\hat{A},\hat{B}]/2} \times C_{AB}(\xi_1,\xi_2)e^{-i(\xi_1A'+\xi_2B')}\,. \quad (21)$$

It is evident from eqs. (20,21) that

[‡1] The form of the generalized distribution function derived is sensitive to the manner in which $\exp[i(\xi_1\hat{A}+\xi_2\hat{B})]$ is expanded. For example, if instead of eq. (18), we used the forms $\exp(i\xi_2\hat{B})\exp(i\xi_1\hat{A})\exp(\xi_1\xi_2[\hat{A},\hat{B}]/2)$, $\exp(i\xi_1\hat{A}/2)\times\exp(i\xi_2\hat{B})\exp(i\xi_1\hat{A}/2)$, or $\exp(i\xi_2\hat{B}/2)\exp(i\xi_1\hat{A})\exp(i\xi_2\times\hat{B}/2)$, all of which are equivalent, we would indeed obtain a different form of the generalized distribution function, yet one which obeys the sum rules of eq. (22).

$$\int F(A',B')\,dA' \equiv |\langle B'|\Psi\rangle|^2 = \frac{1}{2\pi}\int d\xi_2 \times C_{AB}(0,\xi_2)\,e^{-i\xi_2 B'} \tag{22a}$$

and

$$\int F(A',B')\,dB' \equiv |\langle A'|\Psi\rangle|^2 = \frac{1}{2\pi}\int d\xi_1 \times C_{AB}(\xi_1,0)\,e^{-i\xi_1 A'} . \tag{22b}$$

Thus, eq. (21) establishes the relationship between the characteristic function for two arbitrary noncommuting observables and the generalized Wigner distribution function. The generalized distribution function has the essential properties of the conventional Wigner function in that an integration of the generalized function over the eigenvalue spectrum of one observable leads to the probability density in the canonically conjugate observable [eq. (22)].

There is no simple probability interpretation of $F(A',B')$ in eqs. (20, 21) because of the necessary overlap between the states of the noncommuting observables. However, if $\hat{A}$ and $\hat{B}$ are made to commute so that $|A'\rangle$ and $|B'\rangle$ are a common set of eigenvectors, then $F(A',B')$ reduces to the probability distribution function for $\hat{A}$ and $\hat{B}$.

Finally, it is noted that the conventional Wigner distribution function for observables $\hat{A}$ and $\hat{B}$ is obtained from

$$P_W(A',B') = \frac{1}{(2\pi)^2}\int d\xi_1 \int d\xi_2 \times C_{AB}(\xi_1,\xi_2)\,e^{-i(\xi_1 A' + \xi_2 B')} , \tag{23}$$

with $C_{AB}(\xi_1\xi_2)$ defined in eq. (16), whereas the alternative distribution function, $F(A',B')$, introduced in eqs. (20, 21) differs from the Wigner function due to the presence of the phase factor $e^{\xi_1\xi_2[\hat{A},\hat{B}]/2}$ in the integrand of eq. (21). For $\hat{A} = \hat{x}$ and $\hat{B} = \hat{p}$, $\hat{P}_W(x,p)$ in eq. (23) reduces to the Wigner function of eq. (2), whereas $F(x,p)$ defined from eq. (20) becomes

$$F(x,p) = \frac{1}{2\pi\hbar}\int_{-\infty}^{\infty} dy\, \Psi^*(x)\Psi(x-y)\,e^{ipy/\hbar} \equiv (2\pi\hbar)^{-1/2}\,\Psi^*(x)\,e^{ipx/\hbar}\,\phi(p) , \tag{24}$$

where $\phi(p)$ is defined in eq. (3b). It is evident that there is a family of functions which are bilinear in Ψ yet satisfy the sum rules of eqs. (3a, b).

There are some interesting questions to be resolved concerning the uniqueness and positive definiteness of Wigner-type quantum distribution functions. Nevertheless, these distribution functions serve a useful purpose for calculating quantum mechanical observables in transport [5] studies and numerous solid-state [8,9] problems.

References

[1] E.P. Wigner, Phys. Rev. 40 (1932) 749.
[2] R.F. O'Connell and E.P. Wigner, Phys. Lett. 83A (1981) 145.
[3] G.J. Iafrate, H.L. Grubin and D.K. Ferry, Bull. Am. Phys. Soc. 26 (1981) 458.
[4] H.L. Grubin, D.K. Ferry, G.J. Iafrate and J.R. Barker, in: VLSI electronics: microstructure science, ed. N.G. Einspruch (Academic Press, New York) to be published.
[5] G.J. Iafrate, H.L. Grubin and D.K. Ferry, J. de Phys. Coll. C7 (1981) to be published.
[6] J.E. Moyal, Proc. Cambridge Philos. Soc. 45 (1949) 99.
[7] A. Messiah, Quantum mechanics, Vol. 1 (Interscience, New York, 1961) p. 442.
[8] G. Niklasson, Phys. Rev. B10 (1974) 3052.
[9] F. Brosens, L.F. Lemmens and J.T. Devreese, Phys. Stat. Sol. (b)81 (1977) 551.

CONSIDERATIONS ON THE FINITE, VERY-SMALL SEMICONDUCTOR DEVICE AND SUPERLATTICE ARRAYS

David K. Ferry, Robert O. Grondin, and
Robert K. Reich
Colorado State University, Fort Collins, CO

Harold L. Grubin
Scientific Research Associates, Glastonbury, CT

Gerald J. Iafrate
Electronics Technology and Device Laboratory
Fort Monmouth, NJ

ABSTRACT

The size of expected future very-small devices will result in their being strongly coupled to the environment in which they are located. In this paper, we examine several of the limitations on the device physics that can be expected to arise in these structures, including the role of the environment and its effect on ballistic transport. In addition, we look at submicron arrays of devices in a lateral surface superlattice (LSSL) and examine transport in such an LSSL through a Wigner function and Monte Carlo approach.

INTRODUCTION

Many people have examined the limit to which semiconductor devices can be scaled downward[1-3]. While small devices in the range 0.1 - 0.3 μm gate length have been made[4], problems such as interconnections, electromigration and thermomigration of metallization, and power density within the device strongly affect the packing density and device size that can be achieved[5]. Yet, no one has evaluated the operation and performance of very-small semiconductor devices, i.e. those that can be conceived in the sub-0.1 μm size range, and the interactions within arrays of such devices. One reason for this is that the transport within such a device cannot be treated in isolation. Because of the size of such a very-small device, it is coupled strongly

to the environment in which it is located. The basic transport equations cannot be separated from their casual boundary conditions and both of these factors must be modified to account for the influence of the device environment[6]. In previous work, some of us have presented a formalism to address this[4,7], but this formalism remains untried due to its inherent complexity. In the present work, we wish to examine qualitatively several of the limitations on the device physics that can be expected to arise in the very-small semiconductor device, particularly with respect to the finiteness of source and sink regions, contact regions and barriers, and the influence of these latter quantities on the ballistic transport that may exist in the device[8,9]. In particular, we examine these effects through the use of discrete area-preserving phase-space maps which display the characteristics of transport in a generic device. In addition, we treat the cooperative interactions that can arise in densely packed arrays of devices.

BALLISTIC TRANSPORT

Potential barriers within the device can play a significant role in the quantum ballistic transport of carriers through it. Such barriers are found in very-small devices, for example, to confine carriers to the active region[3], and are an intimate part of devices such as the planar-doped barrier transistor[10], tunneling barrier devices[11], real-space transfer devices[12], or superlattice avalanche photodiodes[13]. When a barrier is present at the contact region, care must be taken to adequately handle turning-point reflection of the electrons from this barrier. Even when the electron has sufficient energy to pass over the barrier, there is a well-known quantum mechanical reflection at the barrier interface. If the potential barrier is smooth, i.e. introduces a transition over many wavelengths, the reflection and wave function matching can be handled by well-known approximation techniques such as the WKB approximation[14], in which the potential barriers represent turning points for a near-classical path. In the very-small device, however, the barriers are expected to be sharp on the scale of the electron wavelength and care must be exercised in matching wavefunctions and determining reflections. The reflection problem is further complicated in real-space transfer devices[12] due to the different band structure on either side of the barrier. Here, additional terms arise due to the spatial variation of the effective mass.

If the potential barriers are slowly varying on the scale of the wave packet, the trajectories are largely those of the classical motion. Even if this is not the case, as we expect for the very-small device, nearly semiclassical trajectories can be expected if the variation of the action is limited to a few low-order derivatives[15]. In semi-classical systems, the phase space of the classical motion forms a natural framework in which to examine problems such as these.

While classical one-dimensional transport appears to be basically simple, there exists recent work that suggests that even this simple problem contains a number of unexpected subtleties[16]. In this paper, we begin to investigate the role of barriers in submicron devices through the use of such finite, area-preserving phase-space mappings of classical dynamics. The use of such mappings reveals a variety of complicated structure[16,17], and has had recent success in explaining the cause of excess noise in Josephson junction parametric amplifiers[18,19]. The results that we obtain indicate that if these mappings are applicable to the VLSI scale, then present concepts of submicron transport may require substantial generalization.

The types of sublet‘es to which we are referring are best illustrated by Fig. 1. There, we are using an area-preserving mapping of particle position (horizontal) and momentum (vertical) within a device active region bounded by two Gaussiam potentials V(x) (overlaid in the figure). In addition, an electric field has been applied.

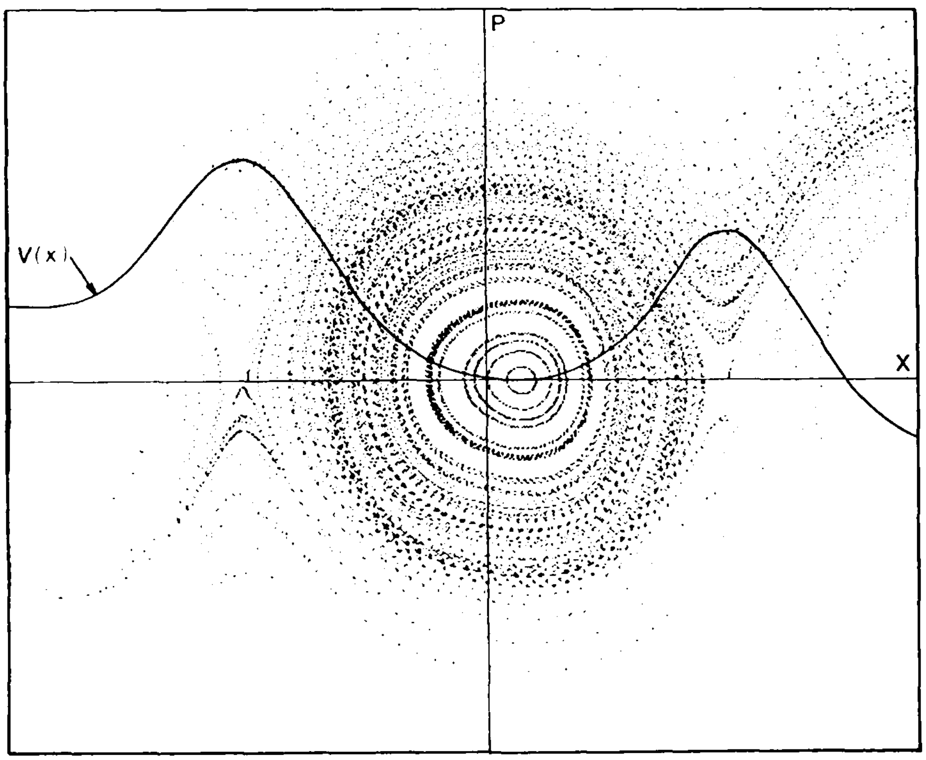

Figure 1. The phase-spacing mapping of an initial uniform distribution of electrons in a generic very-small semiconductor device. The contact regions are represented by a twin-gaussian potential V(x). The horizontal direction is position while the vertical direction is momentum.

The canonical mappings are area-preserving since we are considering a collisionless (conservative) system and looking at the ballistic transport. The classical differential equations of motion are

$$\begin{aligned} \dot{p} &= -\frac{\partial V(x)}{\partial x} , \\ \dot{x} &= + p/m , \end{aligned} \tag{1}$$

and the discreet classical area-preserving maps are

$$\begin{aligned} p_{n+1} &= p_n - T \left.\frac{\partial V}{\partial x}\right|_{x_{n+1}} , \\ x_{n+1} &= x_n + T\, p_n/m . \end{aligned} \tag{2}$$

In Fig. 1, the potential has been scaled so that the two potentials have a weak overlap. For small values of the total energy, resonant orbits occupy the central part of the figure. These orbits are in the region of the classically integrable motion. For larger values of the energy, however, the orbits are such that the particles are swept out of the well by the field. An energy dissipating collision can drop a high energy particle into the resonant region, thus trapping it within the structure. We expect these particles to contribute a diffusive component of current. Large angle scattering, however, can move a particle to a back-flowing orbit, which effectively causes a reflection of particles from the device input.

A number of interesting factors arise. The potential is generic, in the sense that it is similar in form not only to the devices mentioned above, but also to the sinusoidal force term in the Josephson junction devices[18,19]. In the latter case, interaction between devices can lead to a parametric pumping of the potential which yields period-doubling bifurcations and chaotic behavior. The system (2) is not truly generic though, as the set (x,p) are not proper action-angle variables. We have examined the behavior through potential pumping, with dissipation, through replacing the first equation of (2) with

$$p_{n+1} = p_n - T\,\frac{\partial V_o(x_{n+1})}{\partial x} - T\gamma p_n + TF_o \sin(\Omega t_n) , \tag{3}$$

where V_o is the set of Gaussian potentials. The factor γ is an effective damping factor. In Fig. 2, we plot the (F_o,Ω) plane results. The curve is a separatrix below which a stable device results. Above the curve, the device is unstable. No period-doubling bifurcations within a single device are found, contrary to[18].

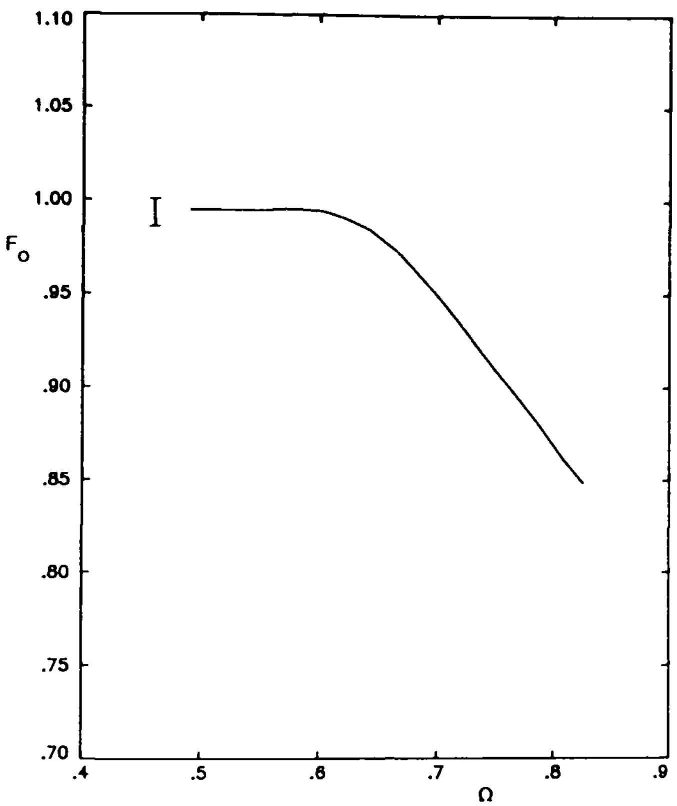

Figure 2. The separatrix in (F_o,Ω) space for parametric pumping of the device of Fig. 1. For values of (F_o,Ω) above the curve, electrons are ejected from the device, while for values below the curve the device is stable.

DEVICE ARRAYS

When device sizes begin to shrink toward the 0.1μm or less region, the line-to-line capacitance in dense device arrays begins to dominate the total node capacitance[4]. This parasitic capacitance leads to a direct device-device interaction outside of the normal circuit or architectural design. In conventional descriptions of LSI circuits, each device is assumed to behave in the same manner within the total system as it does when it is isolated. In the dense arrays discussed here, this will no longer be the case.

The possible device-device coupling mechanisms are numerous and include such effects as the capacitive coupling mentioned above, but also include such effects as wave function penetration or tunneling and charge spill-over. Formally, however, one may describe these effects on system and device behavior by assuming the simplest form of coupling. Arrays of devices, interacting in this manner, form a

lateral surface superlattice[20,21]. Lateral superlattices, in wh the superstructure lies in a surface or heterostructure layer, o considerable advantages for obtaining superlattice effects in pl technology. While a surface MOS structure is formally similar t array of CCD devices[20,22], superlattices can also be fabricated the use of electron and ion beam lithography and selective area taxial growth[21]. If the coupling is capacitive, then the limita to a spacing less than the de Broglie wavelength is removed[4]. W have examined transport in such lateral surface superlattices (L through a Wigner function approach. Before proceeding, however, is worth noting that the circuit theory view of LSSLs[4] is generi that of cellular automata[23]. Many of the image processing appli tions proposed for LSSLs[24] arise from the "games" aspect of cell automata[25].

Superlattice structures give rise to sinusoidal energy mini-bands with relatively narrow widths. The shape of such bands re in interesting electrical transport properties. Lateral surfac superlattices have cosinusoidal bands in two dimensions, with th third dimension quantized with discrete energy levels.

We have calculated the transport properties for such LSSLs a Wigner function formulation. A complete integral equation is tained for the Wigner function and must be solved to obtain the t port coefficients[26,27]. However, the form of the solutions can found by taking the average velocity and energy from the first ar second moments of an equivalent Wigner representation of the tran port equation[28]. A constant electric field is applied in the pla of the sinusoidal bands. For simplicity, a constant relaxation t τ can be used. Solving these two equations simultaneously leads the velocity and energy as functions of the field[29]

$$\langle v_z \rangle = (\varepsilon + \langle E_\perp \rangle - \langle E_o \rangle) \frac{(2\pi/\hbar L)^2 eF_z \tau}{1 + (2\pi eF_z \tau/\hbar L)^2} ,$$

$$\langle E \rangle = \varepsilon + \langle E_\perp \rangle + \frac{\langle E_o \rangle - \varepsilon - \langle E \rangle}{1 + (2\pi eF_z \tau/\hbar L)^2} ,$$

where $L = 2\pi/D$, D is the LSSL spacing, ε is one-half the band-wid and $\langle E_o \rangle$ and $\langle E_\perp \rangle$ are the equilibrium and transverse energies, re spectively.

The velocity as a function of field has the same basic analy expression as that obtained by Lebwohl and Tsu[30] except for the e factor in front of the expression for the field. The difference in effect caused by the different equilibrium distribution chosen In the latter paper, the authors assumed the initial equilibrium

tribution is very close to a zero temperature Fermi-Dirac function, while here the distribution is a finite temperature Wigner distribution and includes the physics of the energy band shape. Note that the velocity as a function of the electric field shows the negative differential mobility predicted earlier and also exhibits the general shape expected of the velocity-field curve.

To more exactly illustrate the mobility and negative differential conductivity, we have carried out a Monte Carlo calculation. The scattering processes are calculated for the model of Iafrate et al.[21], and thus are for the system of GaAs/GaAlAs. The scattering rates for acoustic and polar optical phonons have been obtained using a two dimensional density-of-states for cosinusoidal energy bands. A Van Hove singularity occurring in the density-of-states produces a singularity in the scattering rate, which was removed by including the self-energy corrections due to the phonons in the vicinity of the singularity. The widely-spaced discrete energy levels in the third dimension allows scattering and transport in that direction to be neglected.

In this surface superlattice, as in others, the conduction band splits into subbands. Here the lowest energy subband was nearly flat. Therefore, transport dominantly occurs in the next higher minibands. The satellite valleys and next subband are at energies of 0.2eV and 0.3eV, respectively, above the subband considered. Their contribution to the transport of electrons is insignificant since there are no intermediate energies through which the electrons can scatter to aid population of upper bands.

The overall transport properties of this system are calculated by an ensemble Monte Carlo technique. The results of the simulation are the velocity-field curves and are shown in Fig. 3. The lower curve results for a field applied along one of the (10) basis vectors of the square lattice array of cylinders while in the top curve the field is applied along a (11) direction. At low fields, both curves show a linear region as expected for most structures. At approximately 8-10 kV/cm the curves begin to bend over to the peak near 13 kV/cm. As the field is further increased, the velocity begins to decrease and for this model continues to decrease to zero as the field tends to infinity.

In summary, transport and scattering in a generic surface superlattice structure exhibits a negative differential mobility arising from Bloch oscillations[31]. This surface superlattice negative differential mobility is expected to be useful at much higher frequencies than that due to the conventional Gunn effect. Alternatively, related instabilities may be an ultimate limit on very large scale integration[3,4,22].

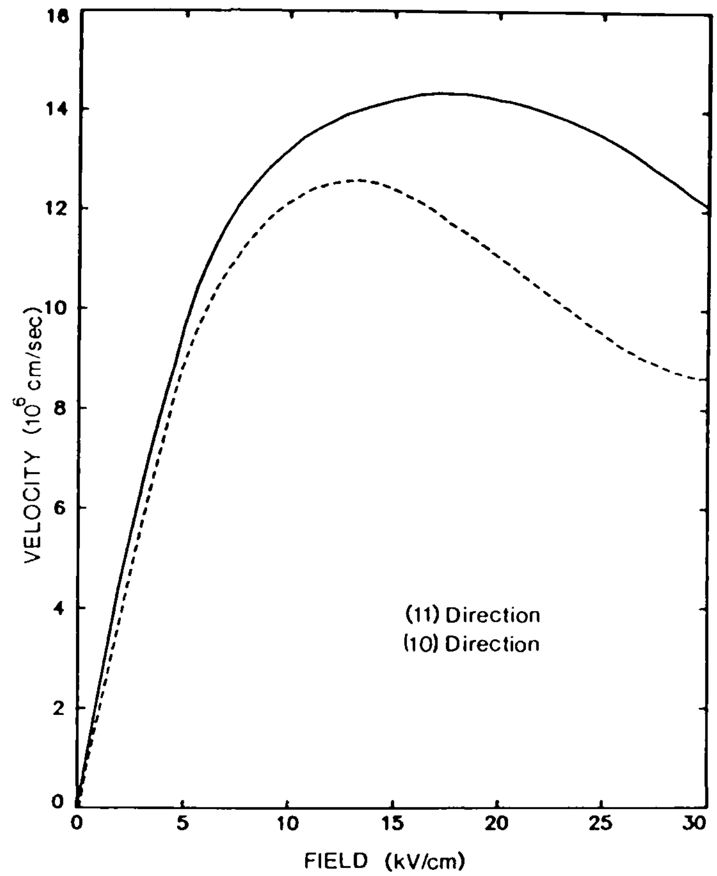

Figure 3. The drift velocity (as a function of electric field) for a LSSL at 300 K. The GaAs/GaAlAs model of ref. 21 has been used.

ACKNOWLEDGEMENT

This work was supported by the Office of Naval Research, the Army Research Office, and the North Atlantic Treaty Organization.

REFERENCES

1. B. Hoeneisen and C. A. Mead, Sol. State Electronics, 15, 819, 891 (1972).
2. J. T. Wallmark, in Inst. of Physics Conf. Series, 25, 133 (1974).
3. J. R. Barker and D. K. Ferry, Sol. State Electronics, 23, 519, 531 (1980).
4. These are reviewed in D. K. Ferry, Adv. in Electronics and Electron Physics, 58, 312 (1982).
5. R. W. Keyes, IEEE Trans. Electron Dev., ED-26, 271 (1979), and references contained therein.

6. M. P. Shaw, H. L. Grubin, and P. R. Solomon, "The Gunn Hilsum Effect", (Academic Press, New York, 1979).
7. J. R. Barker and D. K. Ferry, in "Proc. IEEE Conf. on Cybernetics, Science, and Society", 1979, pp. 762-5 (IEEE Press CH1424-1, 1979).
8. J. R. Barker, D. K. Ferry, and H. L. Grubin, IEEE Electron Dev. Letters, EDL-1, 209, (1980), and references contained therein.
9. D. K. Ferry, J. Zimmermann, and P. Lugli, IEEE Electron Dev. Letters, EDL-2, 228, (1981). See also the papers in IEEE Trans. Electron Devices, August (1981).
10. R. J. Malik, M. A. Hollis, L. F. Eastman, D. W. Woodard, C. E. C. Wood, and T. R. AuCoin, in Proc. Eighth Biennial Cornell Electr. Engr. Conf., Ithaca, N.Y., (1981).
11. P. A. Blakely, J. R. East, and G. I. Haddad, "Tunneling Transistors for Millimeter-Wave Operation", submitted for publication.
12. M. Keever, H. Shichijo, K. Hess, S. Banerjee, L. Witkowski, H. Morkoc, and B. G. Streetman, Appl. Phys. Letters, 38, 36, (1981).
13. F. Capasso, W. T. Tsang, A. L. Hutchinson, and G.F. Williams, Applied Physics Letters, 40, 38, (1982).
14. See, e.g., L. I. Schiff, "Quantum Mechanics", Third Ed., (McGraw-Hill, New York, 1968), pp. 269-79.
15. L. S. Schulman, "Techniques and Applications of Path Integration", (Wiley-Interscience, New York, 1981).
16. See, e.g., "Topics in Nonlinear Dynamics", Ed. by S. Jorna, A.I.P. Conf. Proc. 46 (American Institute of Physics, New York, 1978).
17. V. I. Arnold and A. Avez, "Ergodic Problems of Classical Mechanics", (Benjamin, New York, 1968).
18. B. A. Huberman, Applied Physics Letters, 37, 750, (1980).
19. N. F. Pedersen and A. Davidson, Applied Physics Letters, 39, 830, (1981).
20. R. T. Bate, Bull. Am. Phys. Soc. 22, 407 (1977).
21. G. J. Iafrate, D. K. Ferry, and R. K. Reich, Surf. Sci. 113, 485 (1982).
22. D. K. Ferry, Phys. Stat. Sol. (b) 106, 63 (1981).
23. A. W. Burks, "Essays on Cellular Automata" (Univ. Illinois Press, Urbana, 1970).
24. See J. R. Barker, these proceedings.
25. M. Gardner, Scientific American 224, 112 (Feb. 1971).
26. I. B. Levinson, Sov. Phys. JETP 30, 362 (1970).
27. D. K. Ferry, H. L. Grubin, and G. J. Iafrate, "Nonlinear Transport in Semiconductors", (Academic Press, in preparation).
28. G. J. Iafrate, H. L. Grubin, and D. K. Ferry, J. Physique 42, (Suppl. 10) C7-307 (1981).
29. R. K. Reich and D. K. Ferry, Phys. Letters A, in press.
30. P. A. Lebwohl and R. Tsu, J. Appl. Phys. 41, 2664 (1970).
31. R. K. Reich, R. O. Grondin, D. K. Ferry, and G. J. Iafrate, Phys. Letters A, in press.

END
FILMED
4-86
DTIC